Frontal cortical regulation of neurogenesis and cellular proliferation in the ventral subventricular zone

Authors/Affiliations:

Moawiah M Naffaa[1,2,†], Rehan R Khan[2], Chay T. Kuo, Henry H. Yin[1,3,†]

1. Department of Psychology and Neuroscience; Duke University

2. Department of Cell Biology, Duke University, School of Medicine

3. Department of Neurobiology; Duke University School of Medicine

†**Correspondence**:

Moawiah Naffaa moawiah.naffaa@duke.edu

Henry Yin hy43@duke.edu

Key words: postnatal neurogenesis, subventricular zone, frontal cortex, anterior cingulate, subep-ChAT^{+}, neural stem cells proliferation, calretinin

Ethics declarations

The authors declare no competing financial interests.

Summary

Neurogenesis and differentiation of the neural stem cells (NSCs) in the subventricular zone (SVZ) are controlled by cell-intrinsic molecular pathways that interact with extrinsic signaling cues. Here we identified a novel circuit that regulates neurogenesis and cellular proliferation in the lateral ventricle SVZ (LV-SVZ). Our results demonstrate direct glutamatergic inputs from the frontal cortex as well as local inhibitory interneurons, control the activity of distinctive cholinergic neurons in the subependymal zone (subep-ChAT^{+}). *In vivo* optogenetic stimulation and inhibition in this circuit were sufficient to control local SVZ neurogenesis, LV NSCs proliferation, and SVZ cellular divisions in ventral SVZ. These findings shed light on local and distal neural circuit activity-dependent regulation of postnatal and adult SVZ neurogenesis and LV-SVZ cellular proliferation.

34 The rodent subventricular zone (SVZ) of the lateral ventricles (LV) is a major site of
35 postnatal neurogenesis [1]. Neurogenesis in SVZ provides a useful model system for studying
36 neuronal regeneration and tissue remodeling in the adult brain [2,3]. LV neural stem cells (NSCs)
37 divide asymmetrically for self-renewal or differentiate to become transient amplifying
38 intermediate progenitors (TAPs) [4-6]. These intermediate progenitors divide and differentiate into
39 doublecortin-positive neuroblasts [7,8], which migrate to the olfactory bulb (OB) [7,9,10], where they
40 become mature interneurons that are incorporated into the local circuitry [11,12]. The generation of
41 adult-born neurons from the SVZ contributes to experience-dependent plasticity in the postnatal
42 brain [13,14] and plays a critical role in social behavior in rodents [12,15,16].

43 The LV NSCs receive inputs from a variety of sources, including neighboring NSCs,
44 TAPs, and neuroblasts[17,18]. Different neurotransmitters, including GABA, dopamine, and
45 serotonin, released by neurons in different brain regions, are also known to regulate postnatal and
46 adult SVZ neurogenesis [19-24]. However, little is known about the local and distal circuity which
47 directly or indirectly influence the SVZ neurogenesis.

48 Recent work has identified a small population of cholinergic neurons in the
49 subependymal space to the lateral ventricle. These neurons, which express Choline
50 acetyltransferase ($ChAT^+$), can modulate the proliferation of LV NSCs and neuroblasts in an
51 activity-dependent manner [25]. They are unlike neighboring striatal cholinergic interneurons, and
52 release acetylcholine (ACh) into the SVZ niche. We hypothesize that the population of
53 subependymal $ChAT^+$ (subep-$ChAT^+$) neurons in the ventral domain of SVZ is a key node in the
54 neural circuit regulation of SVZ neurogenesis and LV NSCs proliferation. Using neural circuit
55 tracing, electrophysiology and *in vivo* optogenetic strategies, we identified a novel neural circuit
56 involving anterior cingulate glutamatergic projections and local calretinin-positive interneurons

that can regulate the activity of subep-ChAT$^+$ neurons. Consequently, this circuit directly modulate SVZ neurogenesis, activity of LV NSCs proliferation and SVZ cellular divisions in the ventral SVZ. These findings revealed a novel circuitry by which frontal cortical inputs can influence cholinergic signaling in ventral SVZ to modulate neurogenesis and cellular proliferation.

Results

Excitatory and inhibitory presynaptic inputs to the subep-ChAT$^+$ neurons

Unlike striatal cholinergic neurons, subep-ChAT$^+$ neurons do not show tonic activity in the absence of synaptic inputs, suggesting that excitatory inputs are needed to activate these neurons[26]. However, it is currently unknown where the excitatory inputs are generated from and how they influence the activity of subep-ChAT$^+$ neurons. We hypothesized that glutamatergic inputs from cortical projection neurons may provide excitatory drive of the subep-ChAT$^+$ neurons. The cortical neurons mainly express vesicular glutamate transporter 1 protein (VGlut1)[27]. To selectively stimulate these glutamatergic inputs, we crossed *VGlut1-Cre* mice with *ChAT-eGFP* and ChR2-tdTomato transgenic mouse line (*Ai27*) that expresses channelrhodopsin in a Cre-dependent manner[28]. The resulting *VGlut1-Cre; ChAT-eGFP; Ai27* mice express channelrhodopsin in all VGlut1$^+$ neurons **(Fig. 1A)**.

Whole-cell recordings from subep-ChAT$^+$ neurons of *VGlut1-Cre; ChAT-eGFP; Ai27* mice showed robust firing in response to 473-nm light activation of VGlut1$^+$ axon terminals (firing frequency = 5.375 ± 0.324 Hz) **(Fig. 1B)**. In voltage-clamp mode (holding at -60 mV), photo-stimulation evoked excitatory postsynaptic currents (EPSCs) in the subep-ChAT$^+$ neurons.

79 The induced currents can be blocked by glutamatergic receptors blockers AP5 (NMDA receptor
80 antagonist) and CNQX (AMPA receptor antagonist) (Current amplitude = 98.2 ± 10.7 pA, and
81 current latency = 8.6 ± 0.62 ms) **(Fig. 1C)**. These findings demonstrate the existence of cortical
82 glutamatergic inputs that drive and regulate the activity of subep-ChAT$^+$ neurons.

83 To examine the inhibitory drivers of subep-ChAT$^+$ neurons, we crossed VGat-ChR2-
84 eYFP (i.e.: channelrhodopsin expressed in GABAergic neurons) with *ChAT-Cre* and *Ai27*. The
85 result is VGat-ChR2-eYFP*; ChAT-Cre; Ai27* mice which allow recording from subep-ChAT$^+$
86 neurons in animals with channelrhodopsin expressed in all GABAergic neurons **(Fig. 1D)**.
87 Whole-cell recordings from subep-ChAT$^+$ neurons in voltage-clamp mode (holding at -60 mV)
88 and activating VGAT$^+$ axon terminals via 473-nm laser resulted in consistent inhibitory
89 postsynaptic currents (IPSCs). The evoked IPSCs in the subep-ChAT$^+$ neurons were blocked by
90 picrotoxin ($GABA_A$ receptors antagonist) (Current amplitude = 196.1 ± 24.13 pA, and current
91 latency = 4.5 ± 0.88 ms) **(Fig. 1E)**. These results suggest that subep-ChAT$^+$ neurons receive
92 direct GABAergic inputs that manage their release of ACh in the SVZ.

93 **Developing rabies virus strategy for tracing neural circuit**

94 Our initial electrophysiological recording results established the presence of excitatory
95 and inhibitory modulators to the activity of subep-ChAT$^+$ neurons **(Fig. 1F)**. However, it remains
96 unclear exactly where these inputs originated. To answer this question, we generated a Cre-
97 dependent *R26R-FLEX-TVA-2A-RabiesG-2A-tdTomato-FLEX (R26F-RTT)* mice to trace the
98 connectivity of subep-ChAT$^+$ neurons via a single Rabies viral injection **(Fig. 2A & B)**. This
99 new tracing tool allows for expressing TVA, RabiesG and tdTomato in all Cre-expressing
100 neurons. The *R26F-RTT* mice were first tested by injecting EnvA G-deleted Rabies-eGFP virus
101 into the striatum where no nonspecific rabies infections were detected at the injection site

102 **(Extended Fig. 1A & B)**. For examining the specific expression of TVA, RabiesG and tdTomato
103 in Cre-dependent mice, *R26F-RTT* mice were crossed with *chat-Cre, VGat-Cre and D2-Cre* to
104 generate *R26F-RTT; chat-Cre, R26F-RTT; VGat-Cre* and *R26F-RTT; D2-Cre* mice, respectively.
105 In *R26F-RTT; chat-Cre mice,* all ChAT$^+$ neurons were only found to express tdTomato
106 **(Extended Fig. 1C)**, which indicates that *R26F-RTT* mice are selectively expressed in Cre-
107 positive neurons**.** To assess the retrogradely trans-synaptic spread of rabies with *R26F-RTT*,
108 EnvA G-deleted Rabies-eGFP virus was injected into the striatum of *R26F-RTT; VGat-Cre* and
109 *R26F-RTT; D2-Cre* mice **(Extended Fig. 2A & C).** After 7-days, the cortical excitatory neurons
110 in cingulate and secondary motor cortices which are presynaptically connected to the striatal
111 VGat$^+$ and D2$^+$ neurons were found labeled with GFP **(Extended Fig. 2B & D)**. This indicates
112 that rabies can retrogradely spread from Cre-positive VGat$^+$ and D2$^+$ neurons when they are
113 crossed with *R26F-RTT* mice. Together, these results demonstrated that *R26F-RTT* mice can
114 express TVA, RabiesG and tdTomato selectively in Cre-expressing neurons and allows for
115 retrograde presynaptic neuronal tracing.

116 To allow for neural tracing of cholinergic neurons, we generated *ChAT-Cre; R26F-RTT*
117 mice to express TVA receptor, RabiesG protein, and tdTomato in all cholinergic neurons **(Fig.**
118 **2B)**. We first injected EnvA G-deleted rabies-eGFP virus into the striatum of P30 *ChAT-Cre;*
119 *R26F-RTT* mice **(Extended Fig. 3A)**. As the striatal cholinergic neurons receive synaptic inputs
120 from each other[29], an infection of a striatal cholinergic neuron with EnvA G-deleted Rabies-
121 eGFP virus results in polysynaptic labeling of other neighbor striatal cholinergic neurons, which
122 subsequently pass rabies to other connected neurons **(Extended Fig. 3B & C)**. Then, EnvA G-
123 deleted Rabies-eGFP virus was injected into the LV of *ChAT-Cre; R26F-RTT* mice to target
124 subep-ChAT$^+$ neurons, immediately following mannitol injection to disrupt the ependymal layer

125 locally **(Fig. 2C & F)**. Using this strategy, we were able to selectively infect a subep-ChAT$^+$
126 neuron and trace their presynaptic inputs **(Fig. 2D & G)**. The local connectivity of subep-ChAT$^+$
127 neurons and their projections were checked at 7- and 14-days post rabies injection **(Fig. 2D, E, G**
128 **& H)**. Unlike striatal cholinergic neurons, subep-ChAT$^+$ neurons in the SVZ niche are not
129 connected with neighboring striatal cholinergic neurons **(Fig. 2I)**. These results confirm that
130 subep-ChAT$^+$ neurons have distinct neuronal connectivity.

131 **Local presynaptic inhibitory input to subep-ChAT$^+$ neurons**

132 Injection of EnvA G-deleted Rabies-eGFP virus into the LV of *ChAT- Cre; R26F-RTT*
133 mice revealed local GFP$^+$ interneurons adjacent to the infected subep-ChAT$^+$ neurons **(Fig. 3A**
134 **& B)**. While staining for markers of the known inhibitory neurons, colocalization between GFP$^+$
135 interneurons and calretinin (CR) antibody was noticed **(Fig. 3C)**.

136 To test if the CR$^+$ interneurons provide local inhibitory inputs to subep-ChAT$^+$ neurons,
137 we performed whole-cell patch clamp recording from subep-ChAT$^+$ neurons of *Cr-Cre; ChAT-*
138 *eGFP; Ai29* mice **(Fig. 3D)**. A high-chloride internal solution was used to detect inhibitory
139 postsynaptic currents (IPSCs) while holding at -60 mV in voltage clamp. We stimulated local
140 CR$^+$ interneurons with blue light and revealed robust evoked IPSCs, which were completely
141 blocked by picrotoxin (current amplitude = 122.3 ± 9.0 pA, and current latency = 4.9 ± 0.33 ms)
142 **(Fig. 3E)**. Then, we tested for other known inhibitory interneurons expressing calbindin (CB$^+$),
143 somatostatin (SST$^+$) or parvalbumin (PV$^+$) **(Extended Fig. 4A)**. Using whole-cell recording from
144 subep-ChAT$^+$ neurons, an optogenetic stimulation of GABA released from these inhibitory
145 interneurons (i.e.: CB, SST and PV) did not induce IPSCs **(Extended Fig. 4B)**.

146 To further confirm the local CR^+ interneuron inputs to the subep-$ChAT^+$ neurons, we
147 used a Patterned Light Stimulator LED controller (Mightex) to target CR^+ labelled neurons in
148 SVZ wholemount of *Cr-Cre; ChAT-eGFP; Ai29* mice. Focal optogenetic activation of a single
149 CR^+ interneuron generated IPSCs in subep-$ChAT^+$ neuron (current amplitude = 40.14 ± 3.78 pA,
150 and current latency = 4.7 ± 0.4 ms) **(Fig. 3F & G)**. Subsequently, we stained against CR and
151 ChAT using *C57BL/6J* mice, revealing the presence of 2-4 CR^+ interneurons surrounding each
152 subep-$ChAT^+$ neuron in the LV-SVZ **(Fig. 3H & I)**. Together these results confirm that local
153 CR^+ interneurons are the main source of inhibitory inputs to the subep-$ChAT^+$ neuron.

154 **Presynaptic excitatory inputs from cingulate cortex area 1 (Cg1) to subep-$ChAT^+$ neurons**

155 To illuminate long distance connections for subep-$ChAT^+$ neurons in the brain, EnvA
156 rVSV-eGFP (EnvA/RABVG-eGFP) virus[30] was injected into the LV of *ChAT- Cre; R26F-RTT*
157 mice **(Fig. 4A)**. Distal GFP^+ projection neurons from the anterior cingulate cortex area 1 (Cg1)
158 were observed in the ipsilateral hemisphere only **(Fig. 4B)**. To confirm the Cg1 input to subep-
159 $ChAT^+$ neurons, pAAV-CaMKIIa-hChR2(E123A)-mCherry virus was first injected into the Cg1
160 region of *C57BL/6J* mice to express mCherry in the GFP^+ neurons from Figure 4B **(Fig. 4C)**. By
161 tracing their projections in the SVZ region, we observed them adjacent to the subep-$ChAT^+$
162 neurons **(Fig. 4D)**.

163 To functionally examines a monosynaptic input from Cg1 to the subep-$ChAT^+$ neurons, a
164 general ChR2 viral vector (pAAV-CaMKIIa-hChR2(E123T/T159C) -EYFP) was injected into
165 the Cg1 region of *Chat-Cre; Ai9* mice to express ChR2 in the projections of Cg1 neurons **(Fig.
166 4E)**. Optogenetic stimulation of the cingulate cortex projections reliably evoked action potentials
167 in subep-$ChAT^+$ neurons (firing frequency = 2.5 ± 0.327 Hz) **(Fig. 4F)**. Using voltage clamp, the
168 optogenetic stimulation induced reliable EPSCs in subep-$ChAT^+$ neurons which were completely

169 blocked by the glutamate antagonists (AP5 and CNQX) (current amplitude = 64.86 ± 2.424 pA,
170 and current latency = 9.1 ± 0.7 ms) **(Fig. 4G)**. These results confirm the presence of
171 glutamatergic neurons in the ipsilateral Cg1 region that excite subep-ChAT$^+$ neurons.
172 To further confirm the (Cg1-subep-ChAT$^+$) circuit, pAAV-Ef1a-DIO
173 hChR2(E123T/T159C)-mCherry virus was injected into the Cg1 region of *VGlut1-Cre; ChAT-*
174 *eGFP* mice to express ChR2 in Cg1 VGlut1$^+$ neurons **(Fig. 4H)**. In the voltage clamp mode,
175 reliably EPSCs were generated in subep-ChAT$^+$ neurons upon optogenetic stimulation of Cg1
176 VGlut1$^+$ neurons projection **(Fig. 4I, Left)**. The induced EPS currents were completely blocked
177 by AP5 and CNQX, confirming the presence of Cg1 glutamatergic inputs (current amplitude =
178 53.29 ± 2.96 pA, and current latency = 8.7 ± 0.44 ms) **(Fig. 4I, Right)**. These findings show that
179 a specific population of cortical neurons in the Cg1 region provides excitatory drive to subep-
180 ChAT$^+$ neurons.

181 ***Calretinin-Cre (Cr-Cre)* mice label the distal Cg1 excitatory presynaptic input to the subep-**
182 **ChAT$^+$ neurons**

183 After identifying Cg1 glutamatergic input into subep-ChAT$^+$ neurons using rabies neural
184 tracing and electrophysiological recording, (Cg1-subep-ChAT$^+$) circuit was then further tested
185 by injecting AAVrg viruses (i.e.: retrograde tracing using AAV viruses) into LVs of *C57BL/6J*,
186 *VGlut1-Cre* and *CR-Cre* mice. Upon injection of pAAVrg-hSyn-mCherry and pAAVrg-hSyn-
187 DIO-mCherry viruses into LVs of *C57BL/6J* and *VGlut1-Cre* mice, respectively **(Extended Fig.**
188 **5A & C)**, we observed mCherry$^+$ neurons in the ipsilateral Cg1 region **(Extended Fig. 5B & D)**.
189 Surprisingly, injecting pAAVrg-hSyn-DIO-mCherry virus into the LV of *CR-Cre* mice labels
190 neurons in the ipsilateral Cg1 region **(Fig. 5A &B)**. The detected mCherry$^+$ neurons in the Cg1
191 of *C57BL/6J*, *VGlut1-Cre* and *CR-Cre* mice post pAAVrg virus injections and the GFP$^+$ Cg1

192 neurons in **Fig. 4B** are located along the same rostro-caudal axis of the Cg1 region. These
193 findings strongly suggest that the Cg1 presynaptic glutamatergic drivers of subep-ChAT$^+$
194 neurons are calretinin$^+$ (CR$^+$) during the postnatal period.

195 To examine that these Cg1 glutamatergic inputs to the subep-ChAT$^+$ neurons are CR$^+$
196 neurons, whole-cell recordings from subep-ChAT$^+$ neurons were first performed in *Cr-Cre;*
197 *ChAT-eGFP; Ai27* mice **(Fig. 5C)**. In voltage mode at -60 mV, optogenetic stimulation of CR$^+$
198 terminals reliably evoked EPSCs (Current amplitude = 106 ± 6.68 pA, and current latency = 5.13
199 ± 0.44 ms), which were completely blocked by AP5 and CNQX **(Fig. 5D)**. This predicts that the
200 population of Cg1 glutamatergic that drives the activity of subep-ChAT$^+$ neurons are CR$^+$
201 postnatally. To further functionally testing whether these Cg1 excitatory CR$^+$ neurons regulate
202 the activity of subep-ChAT$^+$ neurons, we injected AAV-EF1a-DIO-hChR2(E123T/T159C)-
203 mCherry virus into the Cg1 region of *Cr-Cre; ChAT-eGFP* mice **(Fig. 5E)**. Whole-cell recording
204 from subep-ChAT$^+$ neurons in voltage clamp mode induced EPSCs upon optogenetic stimulation
205 (Current amplitude = 33 ± 2.46 pA, and latency = 5.13 ± 0.44 ms) **(Fig. 5F)**. All previous data
206 confirm that a specific population of cortical neurons in Cg1 region (VGlut1$^+$ and CR$^+$) provides
207 excitatory drive to subep-ChAT$^+$ neurons **(Fig. 5G)**.

208 The total number of labeled Cg1 cortical neurons with *Cr-Cre* mice during postnatal
209 period is must lower than the number of labeled neurons with *VGlut1-Cre* mice. Thereby, the *Cr-*
210 *Cre* mouse is a reliable tool to study the population of glutamatergic neurons from the Cg1
211 region that control the activity of subep-ChAT$^+$ neurons.

212 ***in vivo* (Cg1-subep-ChAT$^+$) circuit stimulation regulate neurogenesis in the ventral domain**
213 **of SVZ**

214 Based on our earlier findings, we defined the Cg1 presynaptic excitatory drivers of
215 subep-ChAT$^+$ neurons. Thereafter, we studied the *in vivo* functional role of (Cg1-subep-ChAT$^+$)
216 circuit on SVZ neurogenesis and LV cellular proliferation. We hypothesized that this circuit
217 regulate SVZ neurogenesis surrounding subep-ChAT$^+$ neurons by modulating the cellular
218 proliferation in the ventral SVZ. To fulfill this aim, AAV-EF1a-DIO-hChR2 (E123T/T159C)-
219 mCherry virus was injected into ipsilateral Cg1, and optical fibers were implanted into the Cg1
220 regions of *Cr-Cre* mice **(Fig. 6A)**. The optogenetic stimulation was continuously conducted for
221 2- or 3-days and delivered by TTL control of 473-nm laser, 10 ms pulses at 10 Hz, lasting 10 s,
222 given once every 1 min **(Fig. 6B and Extended Fig. 6A)**.

223 In the 2-days circuit stimulation experiments, the mice were perfused immediately after
224 stimulation cessation and brain slices of the stimulated Cg1 sections were stained against ChAT,
225 phospho-S6 ribosomal (P-S6) and doublecortin (DCX) antibodies. To confirm (Cg1-subep-
226 ChAT$^+$) circuit activation in the studied coronal sections, the neuronal activity of subep-ChAT$^+$
227 neurons in these sections was determined by quantifying the intensity of P-S6 protein **(Extended**
228 **Fig. 6B (B' & B''); upper)**. Among the included coronal sections in our studies, subep-ChAT$^+$
229 neurons on the ipsilateral side showed significantly higher P-6S intensity than their counterpart
230 on the contralateral side within the same brain (43.9 ± 7.3%) **(Extended Fig. 6C)**. In these
231 sections, the doublecortin (DCX$^+$) neuroblasts surrounding subep-ChAT$^+$ neurons on the
232 activation side were not clustered and were mainly disordered unlike their counterpart DCX$^+$
233 neuroblasts on the contralateral side **(Extended Fig. 6B (B' & B''); lower)**. This observed
234 disorganized pattern of the clustered local DCX$^+$ cells adjacent to the activated subep-ChAT$^+$
235 neurons may be related to the continuous stimulation of the circuit which result in a local
236 constant release of ACh. Although the circuit was stimulated for two days, the quantification of

237 the total number of DCX$^+$ neuroblasts showed no significant difference between the ipsilateral
238 (activated) and contralateral (control) sides of these coronal sections **(Extended Fig. 6D)**. The
239 total DCX$^+$ cells in the whole SVZ were also assessed by quantifying the intensity of DCX
240 staining on the ipsilateral SVZ (stimulated) vs. contralateral SVZ (control) **(Extended Fig. 6E)**.
241 The intensity of DCX was remarkably higher in the activated SVZ compared to the control SVZ
242 (17.7 ± 6.6%) **(Extended Fig. 6F).**

243 In (Cg1-subep-ChAT$^+$) circuit stimulation experiment for 3-days, the neuronal activity of
244 subep-ChAT$^+$ neurons was first examined in the coronal sections which were used for functional
245 studies **(Fig. 6C (C' & C''); upper)**. These sections have shown remarkable higher P-S6
246 intensity in the ipsilateral (activated) subep-ChAT$^+$ neurons compared to the subep-ChAT$^+$
247 neuron in the contralateral (control) side of the same brain (37.8 ± 8.2%) **(Fig. 6D)**. The DCX$^+$
248 neuroblasts surrounding the subep-ChAT$^+$ neurons on the activation side were highly
249 randomized and not clustered as their comparative DCX$^+$ cells on the contralateral side **(Fig. 6C**
250 **(C' & C''); lower (red arrows))**. Due to the persistent stimulation of subep-ChAT$^+$ neurons,
251 constant generation of DCX$^+$ neuroblasts was observed, thus many neuroblasts migrate before
252 they cluster together **(Fig. 6E; red arrows)**. Notably, the higher rate of newly produced DCX$^+$
253 neuroblasts in the activated side compared to the control side led to more accumulation of
254 neuroblasts on the margins of the dorsal and ventral SVZ domains **(Fig. 6E; blue arrows)**. The
255 total number of DCX$^+$ cells in the stimulated coronal section of the ipsilateral side was
256 significantly higher than on the contralateral side (25.2 ± 4.3%) **(Fig. 6F)**. Although, the
257 intensity of DCX staining of the stimulated and control SVZ wholemounts does not appear to be
258 significantly different from each other **(Fig. 6G & H)**, it was observed to be less in the area

259 surrounding subep-ChAT$^+$ neurons of the stimulated ventral SVZ compared to the control ventral
260 SVZ **(Fig. 6G; yellow dotted circle)**.

261 ***in vivo* (Cg1-subep-ChAT$^+$) circuit stimulation regulate cellular proliferation in the ventral**
262 **domain of SVZ**

263 So far, we demonstrated the role of (Cg1-subep-ChAT$^+$) circuit in regulating the activity
264 of ventral SVZ neurogenesis. Subsequently, we studied the impact of this circuit on the regional
265 LV cellular proliferation around subep-ChAT$^+$ neurons in the ventral SVZ. To achieve this goal,
266 AAV-EF1a-DIO-hChR2 (E123T/T159C)-mCherry virus was injected into ipsilateral Cg1, and
267 optical fibers were implanted into the Cg1 regions of *Cr-Cre* mice **(Fig. 7A; right)**. To test the
268 stimulation effect of (Cg1-subep-ChAT$^+$) circuit on the LV-SVZ cellular proliferation, the circuit
269 was activated for one day and 5-Ethynyl-2′-deoxyuridine (EdU) was intraperitoneally (IP)
270 injected within the last 2-3 hours before mice were sacrificed. **(Fig. 7A; left)**. Due to the spatial
271 cellular arrangements of proliferative cells and subep-ChAT$^+$ neurons in the LV-SVZ neurogenic
272 niche, we used SVZ wholemount to observe the cellular proliferation in the V-SVZ (i.e.: the
273 proliferative cells underneath ependymal cells and 4-6um above subep-ChAT$^+$ neurons) and
274 SVZ (i.e.: the proliferative cells lining around the subep-ChAT$^+$ neurons) **(Fig. 7B)**.

275 Prior to observing the cellular proliferation in the area around subep-ChAT$^+$ neurons, we
276 first examined the neuronal activity of subep-ChAT$^+$ neurons in the stimulated SVZ wholemount
277 compared to their counterpart in the control SVZ wholemount. A mouse in each group of the
278 stimulated mice was used to inspect and analyze the neuronal activity of subep-ChAT$^+$ neurons
279 **(Extended Fig. 7A)**. In these devoted mice, the activity of subep-ChAT$^+$ neurons in the
280 stimulated SVZ was higher than in the control ones (31.6 ± 7.8%) **(Extended Fig. 7B)**. A
281 combination of EdU with either GFAP (glial fibrillary acidic protein) or pEGFR (epidermal

282 growth factor receptor (phospho Y1068)) markers were used to view the cellular proliferation
283 adjacent to subep-ChAT$^+$ neurons in the ventral SVZ **(Fig. 7C & E)**. While GFAP$^+$ cells (i.e.: A
284 marker of quiescent NSCs (qNSCs) and early activated NSCs (aNSCs))[6] were observed mainly
285 in the V-SVZ **(Fig. 7C)**, the number of spatially localized EdU$^+$/GFAP$^+$ cells above the subep-
286 ChAT$^+$ neurons in the ipsilateral V-SVZ (activated) **(Fig. 7C')** were higher than in the
287 contralateral V-SVZ (control) **(Fig. 7C'')** (3 ± 0.56%) **(Fig. 7D)**. This shows that (Cg1-subep-
288 ChAT$^+$) circuit regulates the proliferative activity of LV NSCs in the ventral SVZ.

289 pEGFR is a known marker for labeling both the aNSCs and transit amplifying cells
290 (TAC)[6] which was utilized here to study the cellular proliferation in the V-SVZ and SVZ post
291 (Cg1-subep-ChAT$^+$) circuit stimulation **(Fig. E)**. In the ipsilateral V-SVZ, the number of
292 spatially localized EdU$^+$/pEGFR$^+$ cells above the subep-ChAT$^+$ neurons were notably higher
293 than in the control V-SVZ **(Fig. 7E' & E''; upper)** (2.23 ± 0.5%) **(Fig. 7F; left)**. This strongly
294 suggests that (Cg1-subep-ChAT$^+$) circuit has a role in the regulation of LV NSCs activity. In
295 addition, there are more observed EdU$^+$/pEGFR$^+$ cells around subep-ChAT$^+$ neurons in the
296 stimulated SVZ than in control SVZ **(Fig. 7E' & E''; lower)** (1.92 ± 0.43%) **(Fig. 7F; right)**.
297 The presence of more proliferative cells in both the V-SVZ and SVZ following the (Cg1-subep-
298 ChAT$^+$) circuit stimulation proposes that this circuit is involved in modulating the activity of
299 NSCs and cellular division in the LV-SVZ.

300 ***in vivo* (Cg1-subep-ChAT$^+$) circuit inhibition modulate SVZ neurogenesis and LV cellular**
301 **proliferation in the ventral SVZ**

302 Our previous results predicted that the (Cg1-subep-ChAT$^+$) circuit controls neurogenesis
303 and cellular proliferative activity in the ventral domain of LV-SVZ. To further understand the
304 role of this circuit, we hypothesized that *in vivo* optogenetic inhibition of (Cg1-subep-ChAT$^+$)

305 circuit is sufficient to modulate the activity of SVZ neurogenesis around subep-ChAT$^+$ neurons.
306 To achieve that, pAAV_hSyn1-SIO-stGtACR2-FusionRed virus was injected into ipsilateral
307 Cg1, and optical fibers were implanted into the Cg1 regions of *Cr-Cre* mice **(Fig. 8A)**. The
308 inhibition of Cg1 CR$^+$ neurons were continuously conducted for two days and were delivered by
309 TTL control of a 473-nm laser **(Fig. 8B)**. The mice were perfused directly after the circuit
310 inhibition was terminated and brain slices of the targeted sections were stained against DCX,
311 ChAT and P-S6 antibodies. The coronal sections included in our studies showed higher neuronal
312 activity of subep-ChAT$^+$ neurons on the ipsilateral (inhibited) side compared to the activity of
313 subep-ChAT$^+$ neurons on the control side within the same mice brain **(Fig. 8C (C' & C'');**
314 **upper)** (-31.25 ± 9.03%) **(Fig. 8D)**. Adjacent to the subep-ChAT$^+$ neurons on the ipsilateral
315 (inhibited) side, the number of DCX$^+$ neuroblasts were significantly lower than their counterpart
316 on the control side **(Fig. 8C (C' & C''); lower)**. These results indicate that the (Cg1-subep-
317 ChAT$^+$) circuit regulates local neurogenesis in the ventral SVZ. Furthermore, the total number of
318 DCX$^+$ neuroblasts on the ipsilateral side was lower than their comparative neuroblasts on the
319 contralateral ones (-16.4 ± 3.2%) **(Fig. 8E & F)**. All previous findings proposed a crucial role for
320 (Cg1-subep-ChAT$^+$) circuit in managing neurogenesis of areas surrounding subep-ChAT$^+$
321 neurons in the ventral SVZ.

322 Subsequently, the inhibition effect of (Cg1-subep-ChAT$^+$) circuit on the LV-SVZ cellular
323 proliferative activity around subep-ChAT$^+$ neurons was investigated. To accomplish this,
324 pAAV_hSyn1-SIO-stGtACR2-FusionRed virus was injected into ipsilateral Cg1, and optical
325 fibers were implanted into the Cg1 regions of *Cr-Cre* mice **(Fig. 8A)**. The (Cg1-subep-ChAT$^+$)
326 circuit was continuously blocked for one day and EdU injected within the last 2-3 hours before
327 mice were sacrificed **(Fig. 8G).** The neuronal activity of subep-ChAT$^+$ neurons was examined in

328 the ipsilateral SVZ and compared to their counterpart in control SVZ within every studied group
329 of mice as described in the previous section **(Extended Fig. 8A)**. In the used mice for this
330 purpose, the subep-ChAT$^+$ neurons in the ipsilateral SVZ wholemounts have shown remarkably
331 lower activity than their contralateral counterparts (-38.1 ± 7.57%) **(Extended Fig. 8B)**. Upon
332 staining for GFAP and EdU markers, the number of spatially localized EdU$^+$/GFAP$^+$ cells above
333 subep-ChAT$^+$ neurons in the ipsilateral V-SVZ **(Extended Fig. 9A')** was noticeably less than in
334 the control V-SVZ **(Extended Fig. 9A'')** (-1.77 ± 0.55%) **(Fig. 9B)**. This suggests that (Cg1-
335 subep-ChAT$^+$) circuit modulates the proliferative activity of LV-NSCs. Furthermore, both
336 pEGFR and EdU markers were applied together to study the effect of circuit inhibition on the
337 proliferative activity of LV aNSCs and TAC in the V-SVZ and SVZ, respectively. The number
338 of EdU$^+$/pEGFR$^+$ cells that spatially resides over the subep-ChAT$^+$ neurons in the ipsilateral V-
339 SVZ was observably lower than in the contralateral V-SVZ **(Fig. 8H' & H''; upper)** (-2.5 ±
340 0.1%) **(Fig. 8I; left)**. Additionally, the noticed number of EdU$^+$/pEGFR$^+$ cells around subep-
341 ChAT$^+$ neurons in the ipsilateral SVZ was less than in control SVZ **(Fig. 8H' & H''; lower)** (-
342 2.7 ± 0.68%) **(Fig. 8I; right)**. Together, these findings suggest that (Cg1-subep-ChAT$^+$) circuit
343 has regulatory roles on the proliferative activity of NSCs and cellular division in the ventral LV-
344 SVZ.

345

346 **Discussion**

347 Postnatal and adult LV NSCs proliferation and SVZ neurogenesis are known to be
348 modulated by neural activity [18]. Here, we identified a novel circuit controlling SVZ
349 neurogenesis and LV-SVZ cell proliferation in the LV-SVZ. Using a Rabies tracing strategy, we
350 determined the source of presynaptic inputs to the subep-ChAT$^+$ neurons, which are

351 demonstrated to direct LV NSCs proliferation[25]. Our results showed that subep-ChAT$^+$ neurons
352 have a different pattern of neural connectivity than the striatal cholinergic neurons which are
353 connected with their adjacent striatal cholinergic neurons[31]. Interestingly, we found that
354 glutamatergic inputs from a specific VGlut1$^+$ neuronal population in the anterior cingulate cortex
355 area 1 (Cg1) that projects directly to subep-ChAT$^+$ neurons. This is the first identification of a
356 distal cortical input that monosynaptically drives subep-ChAT$^+$ neurons and regulate their
357 activity in the SVZ niche. In addition, we also identified a small population of local GABAergic
358 calretinin (CR$^+$) interneurons that directly inhibit subep-ChAT$^+$ neurons. Previously, GABA was
359 shown to be involved in various functions in the SVZ such as enhancing neuroblast maturation
360 [32], and preserving the postnatal/adult LV NSCs by inhibiting their proliferation and
361 differentiation , but the source of GABA was largely unclear [21,33]. We demonstrated here for the
362 first time GABAergic CR$^+$ interneurons are a local source of GABA. Future studies may reveal
363 the neuronal connectivity of these distinct local CR$^+$ interneurons and other roles in the LV-SVZ
364 cell proliferation and neurogenesis processes.

365 The subep-ChAT$^+$ neurons predominantly reside in the ventral domain of the SVZ. I*n*
366 *vivo* optogenetics stimulation and inhibition of the defined (Cg1-subep-ChAT$^+$) circuit is
367 sufficient to modulate SVZ neurogenesis surrounding the subep-ChAT$^+$ neurons in the ventral
368 area. While this strongly suggests that subep-ChAT$^+$ neurons release ACh locally in the ventral
369 SVZ, further research can be directed to understand their axon terminals in the whole SVZ niche.
370 In consequence, i*n vivo* optogenetics modulation of this circuit is also sufficient to regulate the
371 activity of LV NSCs proliferation and cellular division regionally in the ventral areas of LV-
372 SVZ. Future research may explore the molecular mechanisms of subep-ChAT$^+$ neuronal
373 regulation of the LV NSCs activity and cellular divisions in V-SVZ and SVZ, respectively.

374 Taken together, our results uncover a new neural circuit that allows direct cortical
375 regulation of the LV-SVZ neurogenesis. In humans, there is evidence for active neurogenesis at
376 the wall of the lateral ventricles that generate migratory neuroblasts for up to two years after
377 birth [34], but the circuit mechanism is unknown. The analogous process in rodents may shed light
378 on how the neurogenesis during postnatal brain development is influenced by synaptic inputs and
379 neural activity. At present, how cortical inputs to the SVZ are related to environmental factors
380 and behavior remains unclear, but our results promise to bridge neural circuit activity with
381 neurogenesis and open a new avenue of research into cortical activity dependent SVZ
382 neurogenesis in postnatal and adult animals.

383

384 **Methods**

385 **Animals**

386 All experiments were approved by the Institutional Animal Care and Use Committee at
387 Duke University. Mice were group housed on a standard 12 h light/dark cycle (lights on at 7
388 a.m.) with a controlled average ambient temperature of 21 °C and 45% humidity. The following
389 mouse lines were purchased from JAX*: C57BL/6J* (000664); *VGlut1-Cre* (023527); *ChAT-eGFP*
390 (007902); ChR2*(RCL-hChR2(H134R)/tdT)-D (Ai27)* (012567); *ChAT- Cre* (006410); *Cr-Cre*
391 (010774); *VGat-Cre* (016962); *Cb-Cre* (028532); *SST-Cre* (013044); *PV-Cre* (017320);
392 *Ai9(RCL-tdT)* (007905). We generated the *R26R-FLEX-TVA-2A-RabiesG-2A-tdTomato-FLEX*
393 (*R26F-RTT*) mouse line for rabies monosynaptic circuit tracing **(Fig. 2A)**.

394 **Rabies virus retrograde tracing**

395 An intraventricular approach via a Cre-dependent viral strategy was employed to avoid
396 labeling striatal ChAT$^+$ neurons. In the beginning we used a monosynaptic circuit tracing with
397 Rabies strategy[35] by injecting the first virus into LV of *ChAT-Cre* mice to express TVA, Rabies-
398 G protein, and tdTomato in subep-ChAT$^+$ neurons. The infected subep-ChAT$^+$ neurons were
399 later targeted with the second EnvA G-deleted rabies virus to enable efficient mono-synaptic
400 tracing. It was extremely difficult to infect the same subep-ChAT$^+$ neurons via two separated
401 viral injections. To overcome this obstacle, *R26R-FLEX-TVA-2A-RabiesG-2A-tdTomato-FLEX*
402 *(R26F-RTT)* mice was successfully generated and validated **(Fig. 2A and Extended Figs. 1, 2 &**
403 **3).** These mice allow for monosynaptic tracing of Cre-targeted neurons via a single EnvA G-
404 deleted Rabies-eGFP (Salk, USA) or EnvA rVSV-eGFP (EnvA/RABVG-eGFP) (Salk, USA)
405 viral injections.

406 **Stereotaxic injections**

407 Stereotaxic injections were performed as mice were kept deeply anesthetized in a
408 stereotaxic frame (David Kopf Instruments) with isoflurane. For circuit tracing, rabies virus, 300
409 nL of (EnvA G-deleted Rabies-eGFP or EnvA rVSV-eGFP (Salk, USA)) virus were injected into
410 striatum or lateral ventricle (LV) of P30 *ChAT-Cre; R26F-RTT* mice. Viruses were infused
411 slowly over 10 min into striatum as the following coordinates relative to Bregma (AP: +1, ML ±
412 2.0, DV: 2.2 from brain surface) or LV (AP: +0.8, ML ± 0.65, DV: 2.1 from brain surface) using
413 a microdriver with a 10 μL Hamilton syringe. For electrophysiological testing of Cg1 inputs to
414 the subep-ChAT$^+$ neurons (optogenetic-light stimulation), adeno-associated viral viruses were
415 used for Cre-dependent expression of the excitatory channelrhodopsin. pAAV-CaMKIIa-
416 hChR2(E123A)-mCherry (addgene #35506) (300nl) virus or pAAV-CaMKIIa-
417 hChR2(E123T/T159C)-EYFP (addgene #35509) (300nl) virus were injected into P30 *C57BL/6J*

418 or P30 *ChAT-Cre; R26F-RTT* mice, respectively. Also, pAAV-Ef1a-DIO
419 hChR2(E123T/T159C)-mCherry (addgene #35510) (300nl) virus was injected into P30 *VGlut1-*
420 *Cre; ChAT-eGFP* and P28 *Cr-Cre; ChAT-eGFP* mice. Viruses were infused slowly over 10 min
421 into the Cg1 using the following coordinates relative to Bregma (AP: +0.8, ML ± 0.3, DV: 0.5
422 from brain surface). For pAAV retrograde tracing, pAAVrg-hSyn-DIO-mCherry (addgene
423 #50459-AAVrg) and pAAVrg-hSyn-mCherry (addgene # 114472-AAVrg) viruses (300 nl) was
424 injected into the LV P28 *Cr-Cre*, P30 *C57BL/6J* (P30) and P30 *VGlut1-Cre*. Viruses were
425 infused slowly over 10 min into the Cg1 as the following coordinates relative to Bregma (AP:
426 +0.8, ML ± 0.65, DV: 2.1 from brain surface) .For *in vivo* optogenetic testing of Cg1 inputs to
427 the subep-ChAT^{+} neurons, pAAV-Ef1a-DIO hChR2(E123T/T159C)-mCherry (addgene #35510)
428 (300nl) and pAAV_hSyn1-SIO-stGtACR2-FusionRed (addgene #105677) (300nl) viruses were
429 injected into P28 *Cr-Cre* mice. Viruses were infused slowly over 10 min into the Cg1 (AP: +0.8,
430 ML ± 0.25, DV: 0.5 from brain surface).

431 All viruses were infused slowly for over 10 min using a Nanoject (Drummond Scientific)
432 connected to a glass pipette. The injection pipette was left in place for 10 min post-injection
433 before it was retracted.

434 **SVZ wholemount preparation and whole-cell patch-clamp recording**

435 For electrophysiology experiments both male and female mice (4- to 10-week-old) were
436 used. They were anesthetized with isofluorane, transcardially perfused and then ventricular wall
437 were dissected as SVZ wholemounts in ice-cold NMDG artificial cerebrospinal fluid (ACSF;
438 containing 92 mM NMDG, 2.5 mM KCl, 1.2 mM NaH_2PO_4, 30 mM $NaHCO_3$, 20 mM HEPES,
439 2 mM glucose, 5 mM sodium ascorbate, 2 mM thiourea, 3 mM sodium pyruvate, 10 mM
440 $MgSO_4$, 0.5 mM $CaCl_2$), and bubbled with 5% CO_2/95% O_2. Tissues were then bubbled in same

441 solution at 37 °C for 15 min, transferred to bubbled, modified-HEPES ACSF at 23–25 °C (92
442 mM NaCl, 2.5 mM KCl, 1.2 mM NaH_2PO_4, 30 mM $NaHCO_3$, 20 mM HEPES, 2 mM glucose, 5
443 mM sodium ascorbate, 2 mM thiourea, 3 mM sodium pyruvate, 2 mM $MgSO_4$, 2 mM $CaCl_2$) for
444 at least 45 min before start experimentation. (For NMDG artificial cerebrospinal fluid and
445 modified-HEPES ACSF solutions, pH was adjusted to 7.5 and osmolarity to 290 mOsm).
446 Recordings were performed in submerged chamber, superfused with continuously bubbled
447 ACSF (125 mM NaCl, 2.5 mM KCl, 1.25 mM NaH_2PO_4, 26 mM $NaHCO_3$, 20 mM glucose, 2
448 mM $CaCl_2$, 1.3 mM $MgCl_2$) at 2.5–5 ml/min at 23–25 °C.

449 Patch electrodes with a resistance of 3–6 MΩ were pulled from borosilicate glass
450 capillaries using a horizontal puller (P-97, Sutter-instruments). All subep-$ChAT^+$ neurons used in
451 the electrophysiology recordings were identified by their distinctive morphology from striatal
452 cholinergic neurons, location (within 15-20 μM from LV surface), their non-spontaneous firing
453 activity, and their depolarized resting membrane potentials (~-45 mV). For measuring EPSCs
454 when holding at – 60 mV, the following internal solution was used: 130 mM potassium
455 gluconate, 2 mM NaCl, 4 mM $MgCl_2$, 20 mM HEPES, 4 mM Na_2ATP, 0.4 mM NaGTP and 0.5
456 mM EGTA, pH adjusted to 7.2 with KOH. A 40 μM picrotoxin ((124-87-8), Millipore Sigma)
457 was added in the bath solution in voltage-clamp mode. For measuring inward IPSCs when
458 holding at – 60 mV, we used internal solution containing K-Cl (high Chloride) KCl (135 Mm),
459 HEPES (10 mM), Na2ATP (2mM), NaGTP (0.2 mM), MgCl2 (2 mM), and EGTA (0.1 mM), pH
460 adjusted to 7.2 with KOH. To block glutamatergic transmission, 50 μM DL-AP5 (NMDA
461 antagonist) ((3693/50), R&D Systems) and 50 μM CNQX (AMPA antagonist) ((0190), Tocris)
462 were added in the bath solution in voltage-clamp mode. To block action potentials in the patched
463 cell, the sodium channel blocker QX-314 (10 mM, 552233, Millipore Sigma) was also added.

464 Signals were amplified with Multiclamp 700B (filtered at 10 kHz), digitized with Digidata
465 1440A (20 kHz), and recorded using pClamp 10 software (Axon). Light-activation of
466 channelrhodopsin was achieved using a 473-nm laser (X-Cite exacte) through a 40x objective
467 (Nikon). Action potentials, evoked EPSCs and evoked IPSCs were analyzed using AxoGrapth
468 (AxoGrapth). One or two subep-ChAT$^+$ neurons were recorded per wholemount SVZ. Up to
469 three neurons from each animal were recorded. Measurements were taken as an average of at
470 least five responses to obtain a data point.

471 For focal (targeted) photostimulation of local CR$^+$-IPSCs from subep-ChAT$^+$ neurons, we
472 used Polygon 400 Digital Micromirror Device (Mightex; multiwavelength pattered illuminator)
473 to control the temporal dynamics (the size, shape, intensity, and position) of light inputs. The
474 illumination consisted of a 100 ms light pulse (470-nm) at 50% intensity in the selected area (50
475 μm). The pulse was triggered using a TTL pulse from the Digidata to synchronize the
476 stimulation with electrophysiology. Photostimulation was performed for one fluorescent subep-
477 CR$^+$ neuron presents in the field of view resulted in postsynaptic effects in the recorded neuron.

478 **Immunofluorescence staining and imaging**

479 Preparation of brain tissue for IHC staining was described previously [25]. We used primary
480 antibodies to GFP (#GFP-1020, 1:400, AVES lab), Choline Acetyltransferase Antibody
481 (#AB144P, 1:250, Millipore sigma), tdTomato [16D7] (#EST203, 1:200, Kerafast), RFP (#600-
482 401-379, 1:250, Rockland), Calretinin (#ab702, 1:200, Abcam), calretinin (#6B3, 1:250, Swant),
483 Calretinin (#MCA-3G9, 1:250, EnCor Biotechnology), RFP (#ab62341, 1:200, Abcam),
484 Doublecortin (#AB2253, 1:250, Millipore), Doublecortin (#4604S, 1:200, Cell Signaling
485 Technology), Doublecortin (#MA5-17066, 1:200, ThermoFisher Scientific), EGFR (phospho

486 Y1068) (#ab5644, 1:250, Abcam), EGFR (phospho Y1068) [Y38] (#ab32430, 1:250, Abcam),
487 GFAP (#GFAP, 1:500, Aves Labs). In brief, for circuit tracing and *in vivo* optogenetic
488 experiments, after experiments mice were deeply anesthetized with isoflurane, perfused
489 transcardially with phosphate buffered saline (PBS), followed by 4% PFA in PBS. The perfused
490 brains were removed and postfixed overnight at 4°C in 4% PFA. The fixed brains were either cut
491 into 50 µm coronal sections by Precisionary Instruments VF-500-0Z vibrating microtome or the
492 SVZ wholemounts were dissected. The coronal slices or SVZ wholemounts were incubated in a
493 blocking solution containing 5% donkey serum and TBST for 100 min at room temperature. The
494 sections were then incubated at room temperature overnight in PBS containing 1% donkey serum
495 and antibodies. They were then washed with PBS and incubated with secondary antibodies,
496 Alexa-594 (1:1000, LifeTech) or Alexa-488 (1:1000, LifeTech) or Alexa-647 (1:1000, LifeTech)
497 for 2 h at room temperature, before washing with PBS. The stained sections were counterstained
498 with a 4′,6-diamidino-2-phenylindole solution (DAPI; (D9542) Sigma-Aldrich). After washing
499 four times with TBST, the sections were coverslipped with Fluoromount (Sigma) aqueous
500 mounting medium. Images were taken using Leica SP8 upright confocal microscope (Zeiss) with
501 10 ×, 20 × and 40 × objectives under the control of Zen software (Zeiss). All antibodies used
502 were validated as in previous publications [25,36] or by publications available on vendor websites
503 specific to each antibody.

504 ***In vivo* optogenetic stimulation and inhibition**

505 Cannula targeting the Cg1 region was implanted (AP: +0.9, ML ± 0.25, DV: 0.4 from brain
506 surface) after injecting pAAV-Ef1a-DIO hChR2(E123T/T159C)-mCherry and pAAV_hSyn1-
507 SIO-stGtACR2-FusionRed viruses as described in **Fig. 6A, 7A & 8A**, using implantable mono
508 fiber-optic fiber (200 µm, 0.22 NA, Doric). Protruding ferrule end of cannula was then connected

509 via fiber cord and a rotary coupling joint (Doric) was used to permit free movement. Three to
510 four weeks after viral infection, light-stimulation was delivered by TTL control (Master 8,
511 AMPI) of a 473-nm laser (IkeCool). For *In vivo* optogenetic stimulation, the ipsilateral Cg1
512 region was stimulated for 10 ms pulses (7-9 mW laser power) at 10 Hz, lasting 10 s, given once
513 every 1 min. For *In vivo* optogenetic inhibition, the Cg1 regions in ipsilateral and contralateral
514 sides were continuously stimulated using 3 mW laser power only to study and avoid overheating
515 in the local cortical areas.

516 For ChAT, DCX, EGFR (phospho Y1068) [Y38], GFAP, CR and RFP analyses, 50-µm
517 brain coronal sections were cut and collected by Precisionary Instruments VF-500-0Z vibrating
518 microtome or SVZ wholemounts were dissected. The sections or areas surrounding the
519 activated/inhibited subep-ChAT^{+} neurons were selected for analyses.

520 ***in vivo* EdU labeling**

521 The 5-ethynyl-2'-deoxyuridine (EdU) staining was conducted using EdU Cell
522 Proliferation Kit for Imaging (EdU *in vivo* Kits) (baseclick GmbH, Germany) according to the
523 manufacturer's protocol. EdU was prepared at 50mg/20mL in sterile PBS and used for pulse
524 labeling of adult mice by performing an intraperitoneal (IP) injection of 500 ul dissolved EdU
525 (50mg/kg). The mice were harvested as described in **Fig. 7 and 8**. The intended coronal slices or
526 SVZ wholemounts for EdU labeling were first stained for other antibodies, and then
527 counterstained with DAPI as described in the immunofluorescence staining section.
528 Subsequently, the sections were washed three times with 3% BSA in PBS. Then, incubated for
529 30 minutes in a reaction cocktail containing Deionized water, Reaction buffer, Catalyst solution,
530 Dye Azide and Buffer additive while protected from light. After the reaction cocktail was
531 removed, sections were washed three times with 3% BSA in PBS. They were then mounted in

532 vectashield mounting media (vector laboratories Inc, Burlingame, CA) and imaged by using
533 Leica SP8 upright confocal microscope (Zeiss) as above. All steps were carried out at room
534 temperature.

535 **Quantification and Statistical Analysis**

536 All data are expressed as mean ± SEM and all statistical analyses were performed using a
537 GraphPad Prism (version 8) program. Paired and unpaired t-tests were used for analysis of *in*
538 *vivo* optogenetics stimulation and inhibition studies. $p < 0.05$ was considered statistically
539 significant.

540

541 **Acknowledgements**

542 We thank Scott Soderling and Shawn Je for helpful comments on the manuscript, Transgenic and
543 Knockout Mouse Facility at Duke University for assistance with generation of R26R-FLEX-
544 TVA-2A-RabiesG-2A-tdTomato-FLEX mice, E. Adlaf, J. Erb, B. Asrican, D. Fromme, P. Paez-
545 Gonzalez, K. Abdi, G. Neves, S. Ramamoorthy, J. David and K. Woldemichael for project
546 assistance. This work was supported by NIH grant R01MH105416.

547

548 **Contributions**

549 M.M.N., C.T.K. and H.H.Y. conceived the project and participated in research design. M.M.N.
550 performed all experiments and analyzed data. R.R.K. helped with preparation of SVZ
551 wholemounts for electrophysiology experiments. M.M.N. and H.H.Y wrote the paper.

552

553 **Reference**

554 1 Lim, D. A. & Alvarez-Buylla, A. The Adult Ventricular-Subventricular Zone (V-SVZ) and Olfactory
555 Bulb (OB) Neurogenesis. *Cold Spring Harb Perspect Biol* **8**, doi:10.1101/cshperspect.a018820 (2016).
556 2 Ihrie, R. A. & Alvarez-Buylla, A. Lake-front property: a unique germinal niche by the lateral
557 ventricles of the adult brain. *Neuron* **70**, 674-686, doi:10.1016/j.neuron.2011.05.004 (2011).
558 3 Lazarini, F. & Lledo, P. M. Is adult neurogenesis essential for olfaction? *Trends Neurosci* **34**, 20-
559 30, doi:10.1016/j.tins.2010.09.006 (2011).
560 4 Doetsch, F., Caille, I., Lim, D. A., Garcia-Verdugo, J. M. & Alvarez-Buylla, A. Subventricular zone
561 astrocytes are neural stem cells in the adult mammalian brain. *Cell* **97**, 703-716,
562 doi:10.1016/s0092-8674(00)80783-7 (1999).
563 5 Obernier, K. *et al.* Adult Neurogenesis Is Sustained by Symmetric Self-Renewal and
564 Differentiation. *Cell Stem Cell* **22**, 221-234 e228, doi:10.1016/j.stem.2018.01.003 (2018).
565 6 Codega, P. *et al.* Prospective identification and purification of quiescent adult neural stem cells
566 from their in vivo niche. *Neuron* **82**, 545-559, doi:10.1016/j.neuron.2014.02.039 (2014).
567 7 Lois, C., Garcia-Verdugo, J. M. & Alvarez-Buylla, A. Chain migration of neuronal precursors.
568 *Science* **271**, 978-981, doi:10.1126/science.271.5251.978 (1996).
569 8 Ponti, G., Obernier, K. & Alvarez-Buylla, A. Lineage progression from stem cells to new neurons
570 in the adult brain ventricular-subventricular zone. *Cell Cycle* **12**, 1649-1650,
571 doi:10.4161/cc.24984 (2013).
572 9 Lois, C. & Alvarez-Buylla, A. Long-distance neuronal migration in the adult mammalian brain.
573 *Science* **264**, 1145-1148, doi:10.1126/science.8178174 (1994).
574 10 Luskin, M. B. Restricted proliferation and migration of postnatally generated neurons derived
575 from the forebrain subventricular zone. *Neuron* **11**, 173-189, doi:10.1016/0896-6273(93)90281-
576 u (1993).
577 11 Petreanu, L. & Alvarez-Buylla, A. Maturation and death of adult-born olfactory bulb granule
578 neurons: role of olfaction. *J Neurosci* **22**, 6106-6113, doi:20026588 (2002).
579 12 Imayoshi, I. *et al.* Roles of continuous neurogenesis in the structural and functional integrity of
580 the adult forebrain. *Nat Neurosci* **11**, 1153-1161, doi:10.1038/nn.2185 (2008).
581 13 Livneh, Y., Adam, Y. & Mizrahi, A. Odor processing by adult-born neurons. *Neuron* **81**, 1097-
582 1110, doi:10.1016/j.neuron.2014.01.007 (2014).
583 14 Sakamoto, M. *et al.* Continuous postnatal neurogenesis contributes to formation of the olfactory
584 bulb neural circuits and flexible olfactory associative learning. *J Neurosci* **34**, 5788-5799,
585 doi:10.1523/JNEUROSCI.0674-14.2014 (2014).
586 15 Mak, G. K. & Weiss, S. Paternal recognition of adult offspring mediated by newly generated CNS
587 neurons. *Nat Neurosci* **13**, 753-758, doi:10.1038/nn.2550 (2010).
588 16 Sakamoto, M., Kageyama, R. & Imayoshi, I. The functional significance of newly born neurons
589 integrated into olfactory bulb circuits. *Front Neurosci* **8**, 121, doi:10.3389/fnins.2014.00121
590 (2014).
591 17 Jones, K. S. & Connor, B. Intrinsic regulation of adult subventricular zone neural progenitor cells
592 and the effect of brain injury. *Am J Stem Cells* **1**, 48-58 (2012).
593 18 Obernier, K. & Alvarez-Buylla, A. Neural stem cells: origin, heterogeneity and regulation in the
594 adult mammalian brain. *Development* **146**, doi:10.1242/dev.156059 (2019).
595 19 Bovetti, S., Gribaudo, S., Puche, A. C., De Marchis, S. & Fasolo, A. From progenitors to integrated
596 neurons: role of neurotransmitters in adult olfactory neurogenesis. *J Chem Neuroanat* **42**, 304-
597 316, doi:10.1016/j.jchemneu.2011.05.006 (2011).

598 20 Young, S. Z., Taylor, M. M. & Bordey, A. Neurotransmitters couple brain activity to
599 subventricular zone neurogenesis. *Eur J Neurosci* **33**, 1123-1132, doi:10.1111/j.1460-
600 9568.2011.07611.x (2011).
601 21 Liu, X., Wang, Q., Haydar, T. F. & Bordey, A. Nonsynaptic GABA signaling in postnatal
602 subventricular zone controls proliferation of GFAP-expressing progenitors. *Nat Neurosci* **8**, 1179-
603 1187, doi:10.1038/nn1522 (2005).
604 22 Hoglinger, G. U. *et al.* Dopamine depletion impairs precursor cell proliferation in Parkinson
605 disease. *Nat Neurosci* **7**, 726-735, doi:10.1038/nn1265 (2004).
606 23 Brezun, J. M. & Daszuta, A. Depletion in serotonin decreases neurogenesis in the dentate gyrus
607 and the subventricular zone of adult rats. *Neuroscience* **89**, 999-1002, doi:10.1016/s0306-
608 4522(98)00693-9 (1999).
609 24 Banasr, M., Hery, M., Printemps, R. & Daszuta, A. Serotonin-induced increases in adult cell
610 proliferation and neurogenesis are mediated through different and common 5-HT receptor
611 subtypes in the dentate gyrus and the subventricular zone. *Neuropsychopharmacology* **29**, 450-
612 460, doi:10.1038/sj.npp.1300320 (2004).
613 25 Paez-Gonzalez, P., Asrican, B., Rodriguez, E. & Kuo, C. T. Identification of distinct ChAT(+)
614 neurons and activity-dependent control of postnatal SVZ neurogenesis. *Nat Neurosci* **17**, 934-
615 942, doi:10.1038/nn.3734 (2014).
616 26 Oldenburg, I. A. & Ding, J. B. Cholinergic modulation of synaptic integration and dendritic
617 excitability in the striatum. *Current opinion in neurobiology* **21**, 425-432 (2011).
618 27 Fremeau, R. T., Jr. *et al.* The expression of vesicular glutamate transporters defines two classes
619 of excitatory synapse. *Neuron* **31**, 247-260, doi:10.1016/s0896-6273(01)00344-0 (2001).
620 28 Madisen, L. *et al.* A toolbox of Cre-dependent optogenetic transgenic mice for light-induced
621 activation and silencing. *Nature neuroscience* **15**, 793-802, doi:nn.3078 [pii]

622 10.1038/nn.3078 (2012).
623 29 Lim, S. A., Kang, U. J. & McGehee, D. S. Striatal cholinergic interneuron regulation and circuit
624 effects. *Front Synaptic Neurosci* **6**, 22, doi:10.3389/fnsyn.2014.00022 (2014).
625 30 Beier, K. T., Saunders, A. B., Oldenburg, I. A., Sabatini, B. L. & Cepko, C. L. Vesicular stomatitis
626 virus with the rabies virus glycoprotein directs retrograde transsynaptic transport among
627 neurons in vivo. *Front Neural Circuits* **7**, 11, doi:10.3389/fncir.2013.00011 (2013).
628 31 Schafer, M. K., Eiden, L. E. & Weihe, E. Cholinergic neurons and terminal fields revealed by
629 immunohistochemistry for the vesicular acetylcholine transporter. I. Central nervous system.
630 *Neuroscience* **84**, 331-359, doi:10.1016/s0306-4522(97)00516-2 (1998).
631 32 Young, S. Z. *et al.* NKCC1 knockdown decreases neuron production through GABA(A)-regulated
632 neural progenitor proliferation and delays dendrite development. *J Neurosci* **32**, 13630-13638,
633 doi:10.1523/JNEUROSCI.2864-12.2012 (2012).
634 33 Alfonso, J., Le Magueresse, C., Zuccotti, A., Khodosevich, K. & Monyer, H. Diazepam binding
635 inhibitor promotes progenitor proliferation in the postnatal SVZ by reducing GABA signaling. *Cell*
636 *Stem Cell* **10**, 76-87, doi:10.1016/j.stem.2011.11.011 (2012).
637 34 Sanai, N. *et al.* Corridors of migrating neurons in the human brain and their decline during
638 infancy. *Nature* **478**, 382-386, doi:10.1038/nature10487 (2011).
639 35 Callaway, E. M. & Luo, L. Monosynaptic Circuit Tracing with Glycoprotein-Deleted Rabies
640 Viruses. *J Neurosci* **35**, 8979-8985, doi:10.1523/JNEUROSCI.0409-15.2015 (2015).
641 36 Benner, E. J. *et al.* Protective astrogenesis from the SVZ niche after injury is controlled by Notch
642 modulator Thbs4. *Nature* **497**, 369-373, doi:10.1038/nature12069 (2013).

643

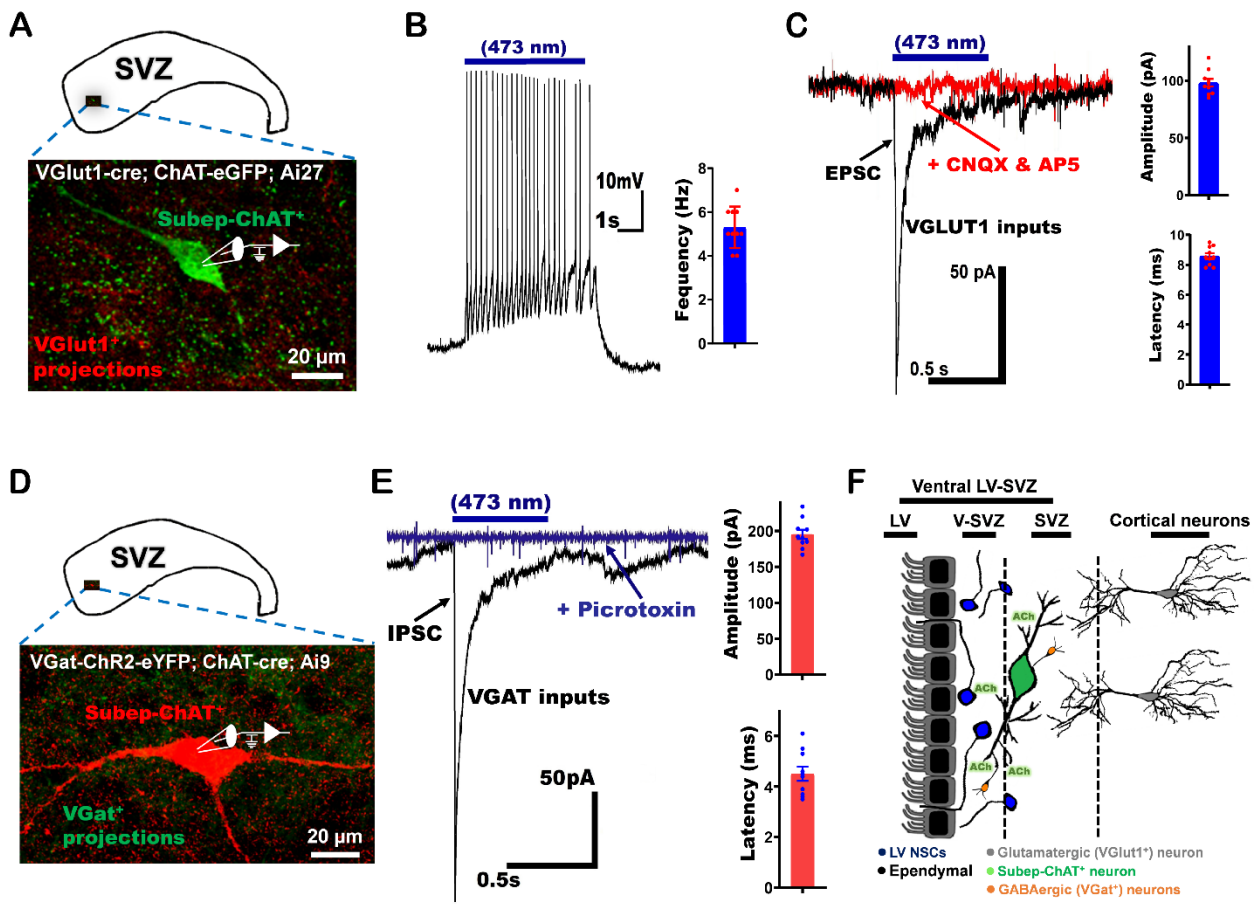

Figure 1 Glutamatergic and GABAergic inputs to subep-ChAT$^+$ neurons.

(A) Illustration of electrophysiological recording of excitatory inputs (VGlut1$^+$) to the subep-ChAT$^+$ neuron from the wholemount of P30-50 *VGlut1-Cre; ChAT-eGFP; Ai27* mice.

(B) Representative trace from whole cell current clamp recording of evoked action potential (APs) from subep-ChAT$^+$ neurons upon blue (473nm) light stimulation for 5s (Left). Blue bar = duration of light stimulation.

Average frequency (Right). $P < 0.0001$, $t_9 = 17.7$, $n = 10$. Data collected from four *VGlut1-Cre; ChAT-eGFP; Ai27* mice. Each dot represents data from one subep-ChAT$^+$ neuron.

(C) Representative trace of EPSCs that were obtained in whole-cell voltage-clamp recordings from subep-ChAT$^+$ neurons after photostimulation for 500ms (black), and the application of AMPA and NMDA receptors antagonists; CNQX and AP-5, respectively (red) (left). Blue bar = duration of light stimulation.

Average evoked EPSC amplitude and latency (Right). $P < 0.0001$, $t_9 = 29.1$, n = 10 and $P < 0.0001$, $t_9 = 44.2$, n = 10, respectively. Data collected from four *VGlut-Cre; ChAT-eGFP; Ai27* mice. Each dot represents the amplitude (upper) and latency (lower) of a single Excitatory Postsynaptic Current (EPSC) recorded from subep-ChAT$^+$ neuron.

(D) Illustration of electrophysiological recording of inhibitory inputs (VGat$^+$) to the subep-ChAT$^+$ neuron from P30-50 *VGat-ChR2-eYFP; ChAT-Cre; Ai9* mice.

(E) Representative trace of electrophysiological recordings of IPSCs that were obtained in whole-cell recordings from subep-ChAT$^+$ neurons upon blue (473nm) light stimulation for 500ms (black), and the application of $GABA_AR$ antagonist; picrotoxin (blue) (left). Blue bar = duration of light stimulation. Each dot represents the amplitude (upper) and latency (lower) of a single Inhibitory Postsynaptic Current (IPSC) recorded from subep-ChAT$^+$ neuron.

Average evoked IPSC amplitude and latency (Right). P value < 0.0001, $t_9 = 30.4$, n = 10 and P value < 0.0001, $t_9 = 16.1$, n = 10, respectively. Data collected from four *VGat-ChR2-eYFP; ChAT-cre; Ai9* mice.

(F) Schematic representation of presynaptic (excitatory and inhibitory) inputs to the subep-ChAT$^+$ neuron.

All error bars indicate SEM

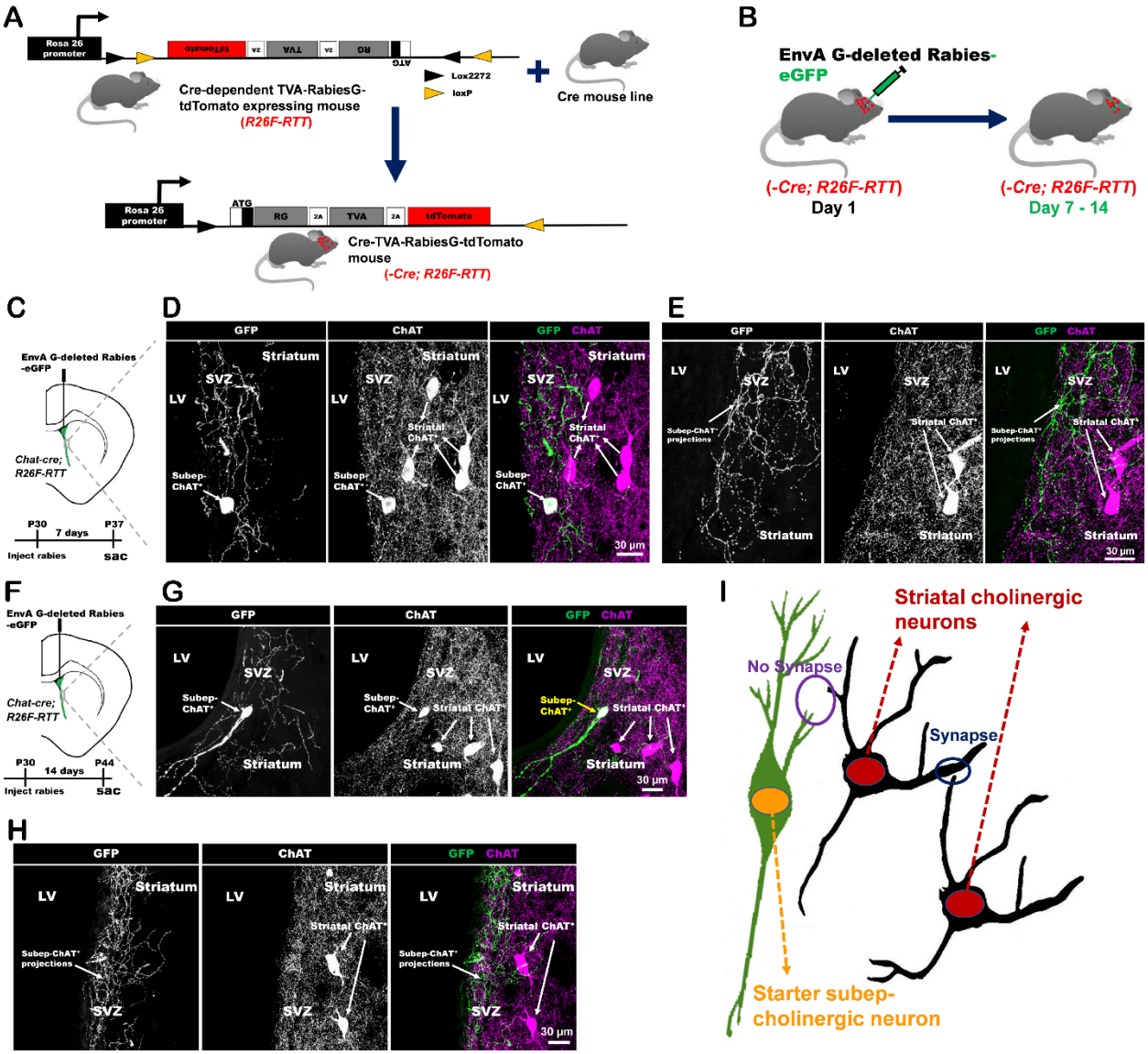

Figure 2 Rabies virus infection of subep-ChAT^{+} neurons.

(A) Schematic representation of *R26R-FLEX-TVA-2A-RabiesG-2A-tdTomato-FLEX* (R26F-RTT) mice before and after Cre recombinase.

(B) Schematic of EnvA G-deleted Rabies-eGFP virus injection into the brain of *-Cre; R26F-RTT* mice.

(C) Experimental representation of EnvA G-deleted Rabies-eGFP virus injection into lateral ventricle (LV) of P30 *Chat-Cre; R26F-RTT* mice. Mice were sacrificed on the day 7 after injection.

(D-E) Immunofluorescence staining for GFP (green) and ChAT (red) in SVZ and striatum of ipsilateral (injected) side of *Chat-Cre; R26F-RTT* mice (7 days post-injection).

686 (F) Experimental representation of EnvA G-deleted Rabies-eGFP virus injection into LV of P30
687 *Chat-Cre; R26F-RTT* mice. Mice were sacrificed on the day 14 after injection.

688 (G-H) Immunofluorescence staining for GFP (green) and ChAT (red) in SVZ and striatum of the
689 ipsilateral (injected) side of *Chat-Cre; R26F-RTT* mice (14 days post-injection).

690 (I) Schematic representation of intra cholinergic connections of striatal cholinergic and subep-
691 $ChAT^+$ neurons.

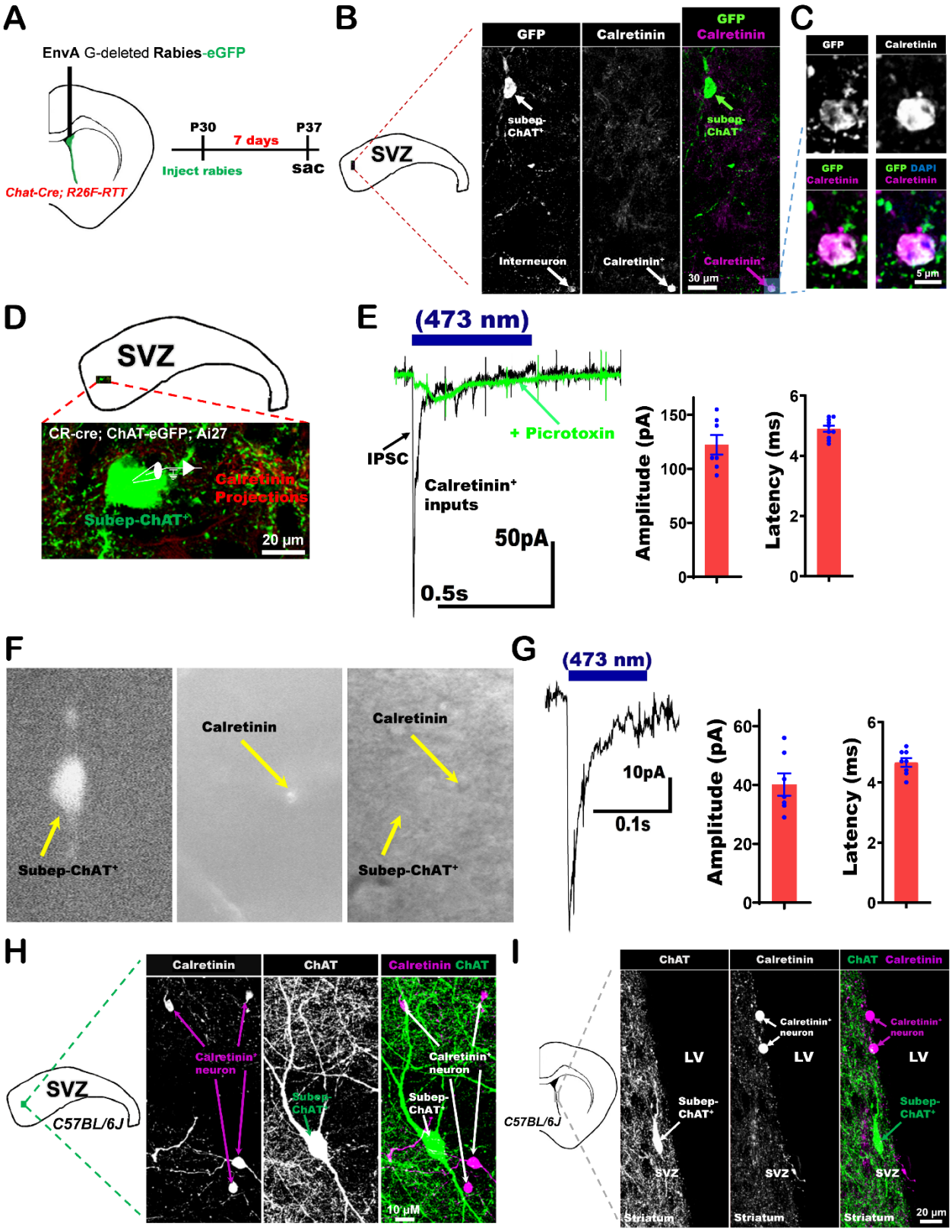

692

693 **Figure 3 Local calretinin-positive (CR$^+$) GABAergic interneurons provide inhibitory inputs**
694 **to subep-ChAT$^+$ neurons.**

(A) Experimental design of EnvA G-deleted Rabies-eGFP virus injection into LV of P30 *Chat-Cre; R26F-RTT* mice.

(B-C) Immunofluorescence staining for GFP (green), Calretinin (purple) and DAPI (blue) in ipsilateral SVZ wholemount (injected) of P37 *Chat-Cre; R26F-RTT* mice.

(D) illustration of electrophysiological recording of calretinin-positive (CR^+) inhibitory inputs to the subep-$ChAT^+$ neurons from SVZ wholemount of P30-50 *Cr-Cre; ChAT-eGFP; Ai27* mice.

(E) Representative trace of evoked IPSCs from subep-$ChAT^+$ neurons upon photostimulation for 500ms (black) and after application of $GABA_AR$ antagonist picrotoxin (green) (Left). Blue bar = duration of light stimulation.

Average current amplitude and latency of the IPSCs upon stimulation (Right). $P < 0.0001$, $t_9 = 19.1$, $n = 10$ and $P < 0.0001$, $t_9 = 46.9$, $n = 10$, respectively. Data collected from five *Cr-Cre; ChAT-eGFP; Ai27* mice. Each dot represents the amplitude (left) and latency (right) of a single Inhibitory Postsynaptic Current (EPSC) recorded from subep-$ChAT^+$ neuron.

(F) Representation of subep-$ChAT^+$ neuron recording from SVZ wholemount of P30-50 *Cr-Cre; ChAT-eGFP; Ai27* mice. Left; subep-$ChAT^+$ neuron (473nm light). Middle; Subep-CR^+ neurons (590nm light). Right; bright field image showing both subep-$ChAT^+$ and -CR^+ neurons.

(G) Representative trace of evoked IPSCs in subep-$ChAT^+$ neurons following photostimulation for 100ms (Left). Blue bar = duration of light stimulation.

Average current amplitude and latency of the IPSCs upon stimulation (Right). $P < 0.0001$, $t_7 = 12.25$, $n = 8$ and $P < 0.0001$, $t_9 = 32.4$, $n = 8$, respectively. Data collected from three *Cr-Cre; ChAT-eGFP; Ai27* mice. Each dot represents the amplitude (left) and latency (right) of an Inhibitory Postsynaptic Current (EPSC) recorded from subep-$ChAT^+$ neuron.

(H-I) Immunofluorescence staining for CR (purple) and ChAT (green) in the SVZ wholemount (H) and coronal section (I) of P28 *C57BL/6J* mice.

All error bars indicate SEM.

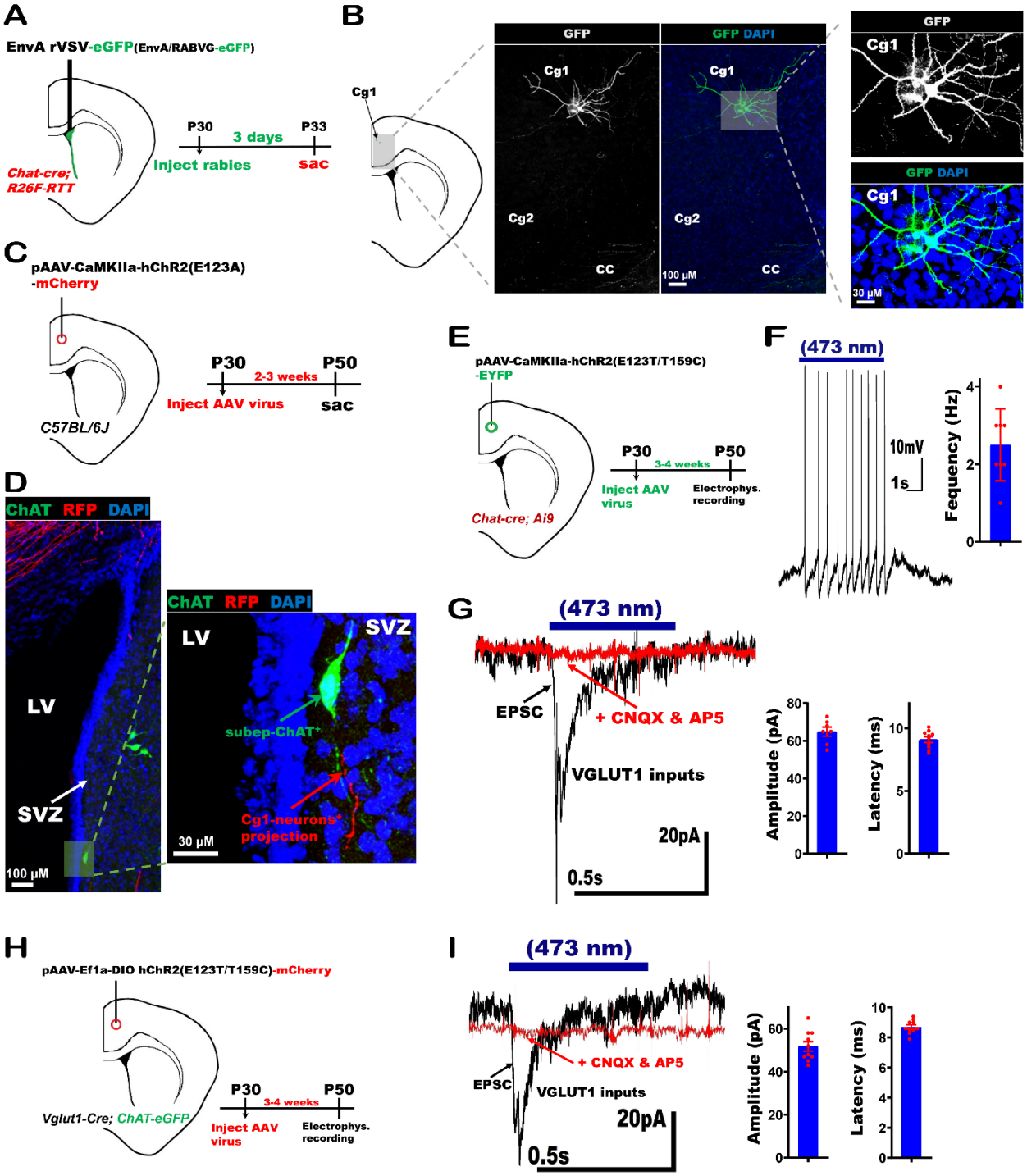

Figure 4 Anterior cingulate cortex projects directly to subep-ChAT^{+} neurons.

(A) Schematic illustration of EnvA rVSV-eGFP (EnvA/RABVG-eGFP) virus injection into LV of P30 *Chat-Cre; R26F-RTT* mice.

(B) A sample of immunofluorescence staining for GFP (green) in anterior cingulate cortex areas 1 and 2 (Cg1 and Cg2) (left) and Cg1 region (right) of ipsilateral (injected) side of P33 *Chat-Cre; R26F-RTT* mice.

(C) Schematic representation of AAV-CaMKII-hChR2(E123A)-mCherry virus injection into Cg1 region of P30 *C57BL/6J* mice.

(D) A sample of immunofluorescence staining for ChAT (green) and infected projections (red) of the ipsilateral Cg1 neurons (injected side) in striatum and SVZ (left), and SVZ (right) of P50 *C57BL/6J* mice in panel C.

(E) Experimental design of pAAV-Ef1a-DIO hChR2(E123T/T159C)-EYFP virus injection into Cg1 region of P30 *Chat-Cre; Ai9* mice. Mice were used for recording 3-4 weeks post-injection.

(F) Representative trace of whole cell current clamp recoding of evoked action potentials (APs) from subep-ChAT$^+$ neurons upon photo-stimulation for 5s (Left). Blue bar = duration of light stimulation.
Average spike frequency (Right). $P < 0.0001$, $t_7 = 7.6$, n = 8. Data collected from five *Chat-Cre; Ai9* mice. Each dot represents data from one subep-ChAT$^+$ neuron.

(G) Representative trace of EPSCs were obtained in whole-cell recordings from subep-ChAT$^+$ neurons upon 473nm light stimulation for 500ms (black), and after blocking with AMPA and NMDA receptors antagonists (CNQX and AP-5, respectively) (red) (Left). Blue bar = duration of light stimulation.
Average EPSC amplitude and latency (Right). P value < 0.0001, $t_9 = 36.16$, n = 10 and P value < 0.0001, $t_9 = 40.5$, n = 10, respectively. Data collected from five *Chat-Cre; Ai9* mice. Each dot represents the amplitude (left) and latency (right) of a single Excitatory Postsynaptic Current (EPSC) recorded from subep-ChAT$^+$ neuron.

(H) Experimental design of pAAV-Ef1a-DIO hChR2(E123T/T159C)-mCherry virus injection into Cg1 region of P30 *VGlut1-Cre; ChAT-eGFP* mice. Mice were used for recording at 3-4 weeks post-injection.

(I) Representative trace of EPSCs were obtained in whole-cell voltage-clamp recordings from subep-ChAT$^+$ neurons upon 473nm light stimulation for 500ms (black), and after blocking with AMPA and NMDA receptors antagonists (CNQX and AP-5, respectively) (red) (Left). Blue bar = duration of light stimulation.
Average evoked EPSC amplitude and latency (Right). P value < 0.0001, $t_9 = 23.3$, n = 10 and P value < 0.0001, $t_9 = 61.2$, n = 10, respectively. Data collected from four *VGlut1-Cre; ChAT-eGFP* mice. Each dot represents the amplitude (left) and latency (right) of a single Excitatory Post Synaptic Current (EPSC) recorded from subep-ChAT$^+$ neuron.

All error bars indicate SEM.

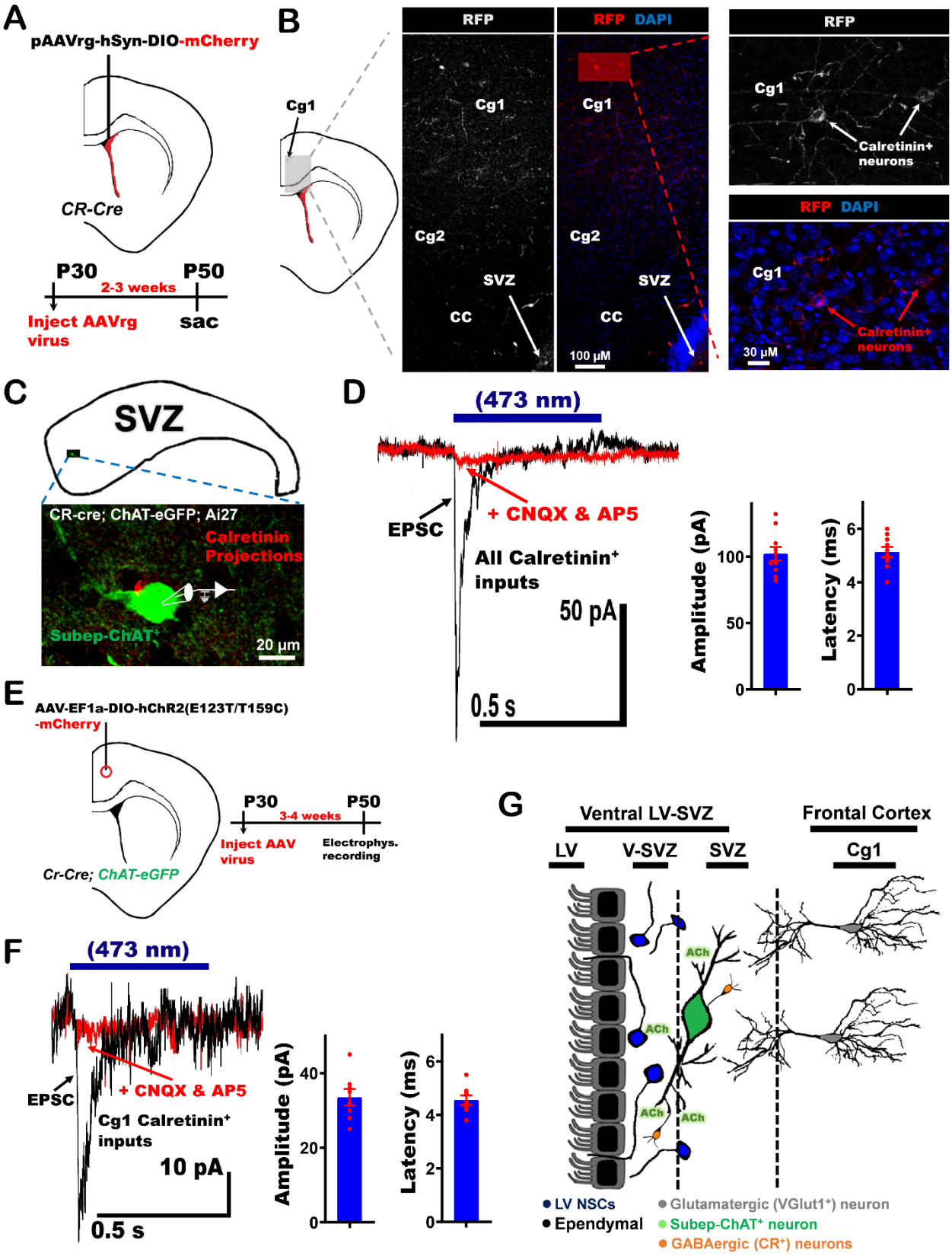
A
pAAVrg-hSyn-DIO-mCherry
CR-Cre
P30
P50
2-3 weeks
Inject AAVrg virus
sac
B
Cg1
RFP
RFP DAPI
Cg1
Cg2
SVZ
CC
100 µM
Calretinin+ neurons
30 µM
C
SVZ
CR-cre; ChAT-eGFP; Ai27
Calretinin Projections
Subep-ChAT+
20 µm
D
(473 nm)
EPSC
+ CNQX & AP5
All Calretinin+ inputs
50 pA
0.5 s
Amplitude (pA)
Latency (ms)
E
AAV-EF1a-DIO-hChR2(E123T/T159C) -mCherry
Cr-Cre; ChAT-eGFP
P30
P50
3-4 weeks
Inject AAV virus
Electrophys. recording
F
(473 nm)
EPSC
+ CNQX & AP5
Cg1 Calretinin+ inputs
10 pA
0.5 s
Amplitude (pA)
Latency (ms)
G
Ventral LV-SVZ
Frontal Cortex
LV
V-SVZ
SVZ
Cg1
ACh
LV NSCs
Ependymal
Glutamatergic (VGlut1+) neuron
Subep-ChAT+ neuron
GABAergic (CR+) neurons

771

Figure 5 Presynaptic cingulate neurons that excite subep-ChAT$^+$ neurons are calretinin-positive (CR$^+$).

(A) Schematic illustration of the experimental design of pAAVrg-hSyn-DIO-mCherry virus injection into LV of P28 *Cr-Cre* mice.

(B) Immunofluorescence staining for RFP (red) in ipsilateral (injected side) anterior cingulate cortex areas 1 and 2 (Cg1 and Cg2) (left) and ipsilateral (injected side) Cg1 region (right) of P50 *Cr-Cre* mice.

(C) Illustration of electrophysiological recording of calretinin-positive (CR$^+$) excitatory inputs to subep-ChAT$^+$ neurons from SVZ wholemount of P30-50 *Cr-Cre; ChAT-eGFP; Ai27* mice.

(D) Representative trace of EPSCs were obtained in whole-cell recordings from subep-ChAT$^+$ neurons upon 473nm light stimulation for 500ms (black), and after blocking with AMPA and NMDA receptors antagonists (CNQX and AP-5, respectively) (red) (Left). Blue bar = duration of light stimulation.
Average EPSC amplitude and latency (Right). $P < 0.0001$, $t_9 = 19.6$, n = 10 and $P < 0.0001$, $t_9 = 27$, n = 10, respectively. Data collected from five *Cr-Cre; ChAT-eGFP; Ai27* mice. Each dot represents the amplitude (left) and latency (right) of a single Excitatory Postsynaptic Current (EPSC) recorded from subep-ChAT$^+$ neuron.

(E) Experimental design of AAV-EF1a-DIO-hChR2(E123T/T159C)-mCherry virus injection into Cg1 of P28 *Cr-Cre; ChAT-eGFP* mice. Mice were used for recording 3-4 weeks post-injection.

(F) Representative trace of EPSCs evoked specifically by Cg1 CR$^+$ input. EPSCs were recorded from subep-ChAT$^+$ neurons of injected mice in panel E upon 473nm light stimulation for 500ms (black). EPSCs were blocked by CNQX and AP-5 (red) (Left).
An average current amplitude and latency (Right). $P < 0.0001$, $t_7 = 15.3$, n = 8 and $P < 0.0001$, $t_7 = 24.9$, n = 8, respectively. Data collected from four *Cr-Cre; ChAT-eGFP* mice. Each dot represents the amplitude (left) and latency (right) of a single Excitatory Postsynaptic Current (EPSC) recorded from subep-ChAT$^+$ neuron.

(G) Schematic summary of (Cg1-Subep-ChAT$^+$) circuit regulation of LV NSCs.

All error bars indicate SEM.

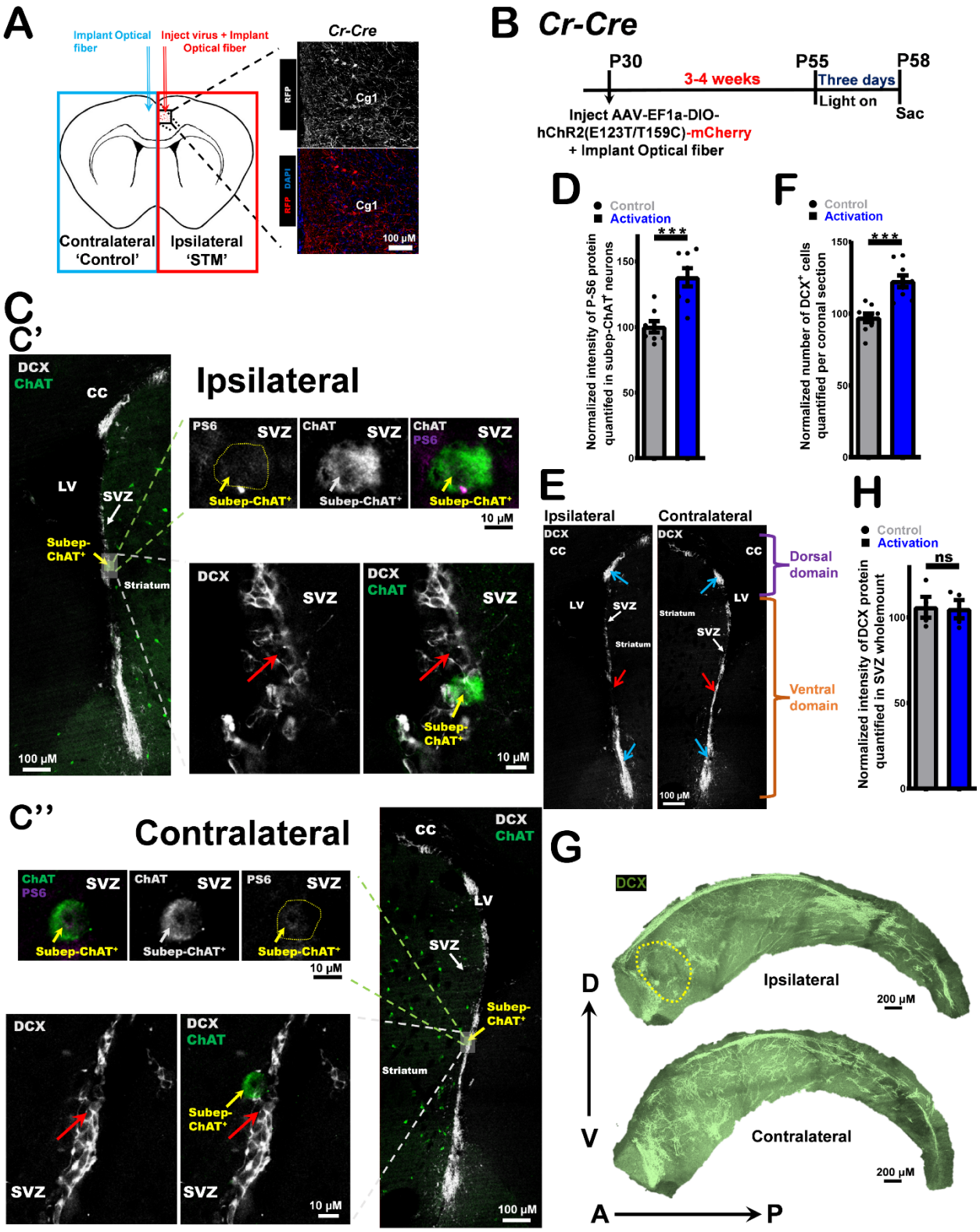

Figure 6 *In vivo* optogenetic (Cg1-subep-ChAT^{+}) circuit stimulation modulates neurogenesis in the SVZ niche.

813 (A) Schematic representation of *in vivo* optogenetic stimulation experiment in panel B.
814 Immunofluorescence staining for RFP (red) in the ipsilateral (injected) Cg1 of *Cr-Cre* mice.

815 (B) Experimental design of *in vivo* optogenetic stimulation for three days post AAV-EF1a-DIO-
816 hChR2(E123T/T159C)-mCherry virus injection into ipsilateral Cg1 and optical fibers
817 implantation into Cg1 regions of P28 *Cr-Cre* mice

818 (C) DCX (grey) and ChAT (green) immunofluorescence staining of (C') ipsilateral (upper images;
819 activation) vs. (C'') contralateral (lower images; control) sides of SVZ from stimulated coronal
820 sections of mice in panel B. Identical settings from same brain section were used for imaging. Red
821 arrows represent DCX^+ neuroblasts around subep-$ChAT^+$ neurons.

822 (D) P-S6 intensity analysis of subep-$ChAT^+$ neurons in ipsilateral side (activation) vs. contralateral
823 side (control). $P<0.0004$, n=8, Paired t-test. Data collected from three stimulated *Cr-Cre* mice.
824 Each dot represents a subep-$ChAT^+$ neuron.

825 (E) DCX (grey) immunofluorescence staining of ipsilateral SVZ (left image; activation) vs.
826 contralateral SVZ (right image; control) from stimulated coronal section of mice in panel C.
827 Identical settings from same brain section were used for imaging. Blue arrows display DCX^+
828 neuroblasts in dorsal (upper) and ventral (lower) domains. Red arrow displays DCX^+ neuroblasts
829 adjacent to subep-$ChAT^+$ neurons in ventral domain of the stimulated SVZ (left) and control SVZ
830 (right).

831 (F) Analysis of DCX^+ neuroblasts in stimulated coronal sections of ipsilateral side (activation) vs.
832 contralateral side (control). $P<0.0001$, n=9, Paired t-test. Data collected from four stimulated *Cr-*
833 *Cre* mice. Each dot represents a total DCX^+ cells per coronal section.

834 (G) DCX (green) immunofluorescence staining of ipsilateral (upper images; activation) vs.
835 contralateral (lower images; control) of SVZ wholemount from stimulated mice in panel B.
836 Identical settings from same brain wholemounts were used for imaging. Yellow dotted circle
837 represents an area where subep-$ChAT^+$ neurons mainly reside in the ventral region of SVZ.

838 (H) Analysis of DCX intensity in ipsilateral SVZ wholemount (activation) vs. contralateral SVZ
839 wholemount (control). $P = 0.766$ (ns), n=4, Paired t-test. Data collected from four stimulated *Cr-*
840 *Cre* mice. Each dot represents a total DCX protein per SVZ wholemount.

841 All error bars indicate SEM.

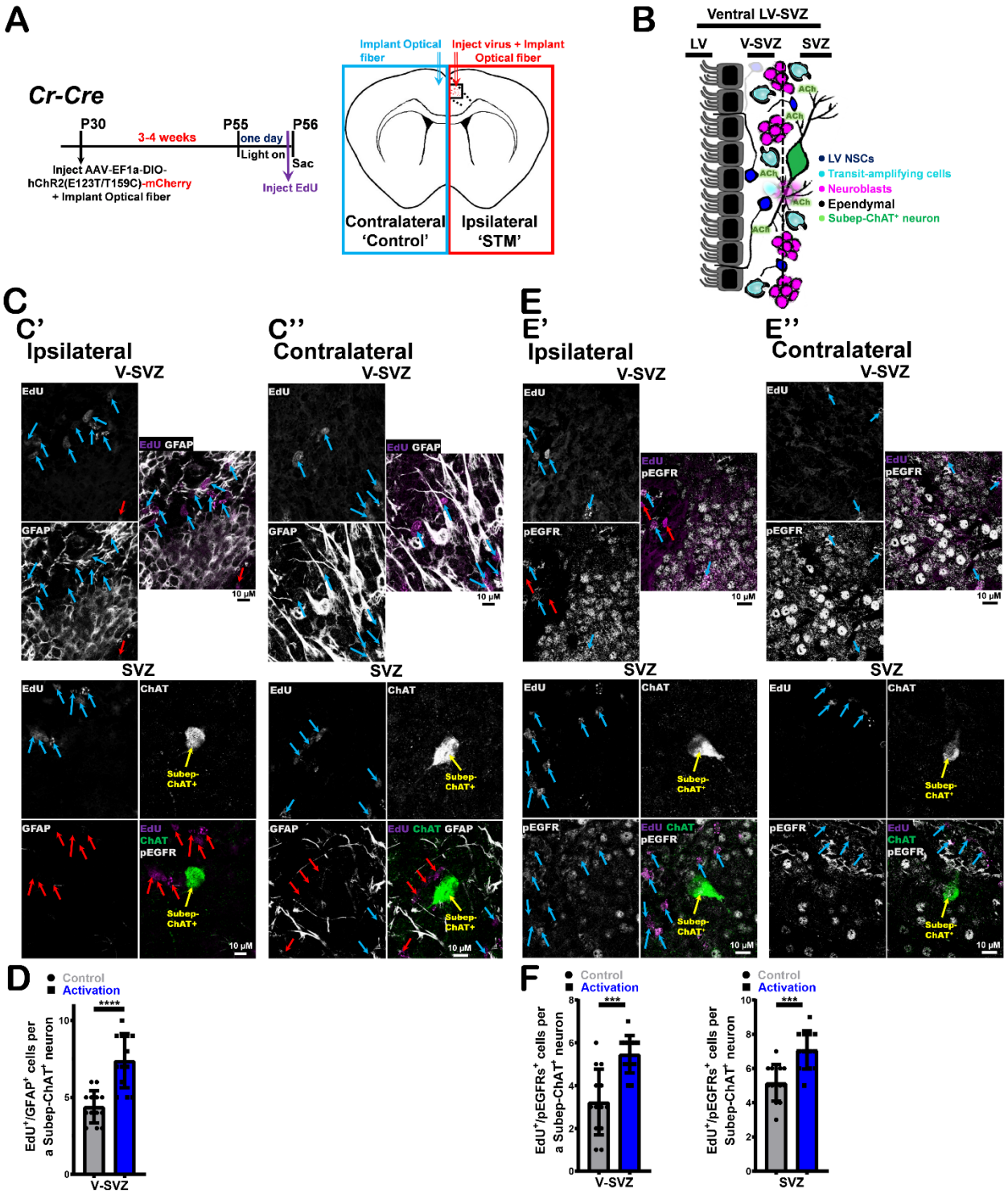

Figure 7 *In vivo* optogenetic (Cg1-subep-ChAT^{+}) circuit stimulation modulates cellular proliferation in the SVZ niche.

(A) Experimental design of *in vivo* optogenetic stimulation for one day post AAV-EF1a-DIO-hChR2(E123T/T159C)-mCherry virus injection into ipsilateral Cg1 and optical fibers implantation into Cg1 regions of P28 *Cr-Cre* mice

(B) Schematic representation of the cellular composition and organization of the LV-SVZ.

(C) EdU (purple), ChAT (green) and GFAP (grey) immunofluorescence staining of (C') ipsilateral SVZ wholemount (activation) (upper images; V-SVZ and lower images; SVZ) vs. (C'') contralateral SVZ wholemount (control) (upper images; V-SVZ and lower images; SVZ) from stimulated mice in panel A. Identical settings from same brain section were used for imaging. Blue arrows display $EdU^+/GFAP^+$ cells surrounding subep-$ChAT^+$ neurons in V-SVZ. Red arrows display $EdU^+/GFAP^-$ cells surrounding subep-$ChAT^+$ neurons in V-SVZ and SVZ.

(D) Analysis of $EdU^+/GFAP^+$ cells in ipsilateral (activation) V-SVZ vs. contralateral (control) V-SVZ of SVZ wholemounts. $P<0.0001$, n=13, Unpaired t-test. Data collected from four stimulated *Cr-Cre* mice. Each dot represents total $EdU^+/GFAP^+$ cells surrounding a subep-$ChAT^+$ neuron.

(E) EdU (purple), ChAT (green) and pEGFR (grey) immunofluorescence staining of (E') ipsilateral SVZ wholemount (activation) (upper images; V-SVZ and lower images; SVZ) vs. (E'') contralateral SVZ wholemount (control) (upper images; V-SVZ and lower images; SVZ) from stimulated mice in panel A. Identical settings from same brain section were used for imaging. Blue arrows display $EdU^+/pEGFR^+$ cells surrounding subep-$ChAT^+$ neurons in V-SVZ and SVZ. Red arrows display $EdU^+/pEGFR^-$ cells surrounding subep-$ChAT^+$ neurons in V-SVZ.

(F) Left: Analysis of $EdU^+/pEGFR^+$ cells in ipsilateral (activation) V-SVZ vs. contralateral (control) V-SVZ of SVZ wholemounts. $P = 0.0001$, n=13, Unpaired t-test. Data collected from four stimulated *Cr-Cre* mice. Each dot represents total $EdU^+/pEGFR^+$ cells surrounding a subep-$ChAT^+$ neuron.

Right: Analysis of $EdU^+/pEGFR^+$ cells in ipsilateral (activation) SVZ vs. contralateral (control) SVZ of SVZ wholemounts. $P = 0.0002$, n=13, Unpaired t-test. Data collected from four stimulated *Cr-Cre* mice. Each dot represents total $EdU^+/pEGFR^+$ cells surrounding a subep-$ChAT^+$ neuron.

All error bars indicate SEM.

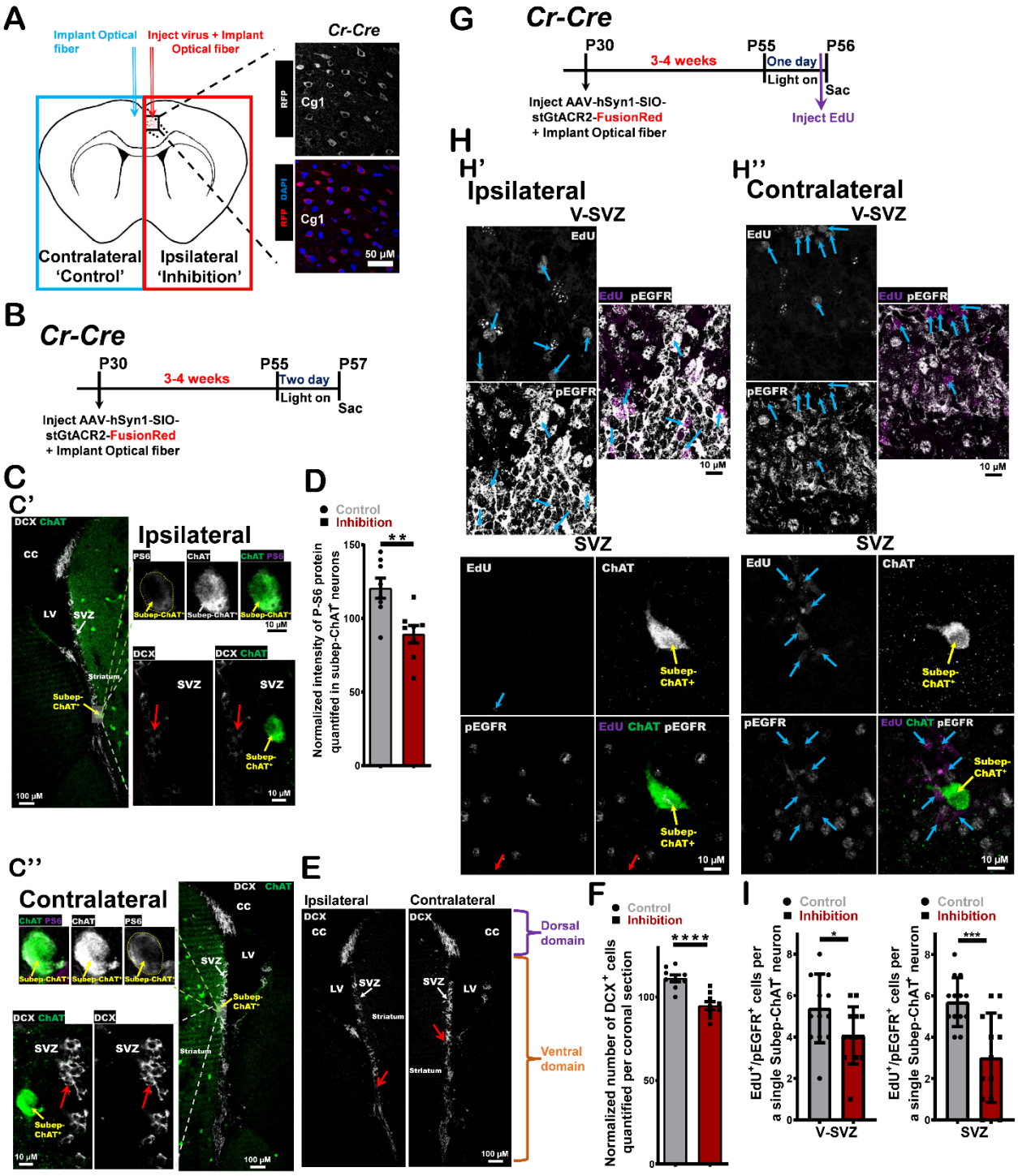

Figure 8 *In vivo* optogenetic (Cg1-subep-ChAT$^+$) circuit inhibition modulates neurogenesis and cellular proliferation in the SVZ niche.

(A) Schematic representation of *in vivo* optogenetic inhibition experiment in panel B. Immunofluorescence staining for RFP (red) in ipsilateral (injected) Cg1 of *Cr-Cre* mice.

881 (B) Experimental design of *in vivo* optogenetic inhibition for two days post AAV_hSyn1-SIO-
882 stGtACR2-FusionRed virus injection into ipsilateral Cg1 and optical fibers implantation into Cg1
883 regions of P28 *Cr-Cre* mice.

884 (C) DCX (grey) and ChAT (green) immunofluorescence staining of (C') ipsilateral (upper images;
885 inhibition) vs. (C'') contralateral (lower images; control) sides of SVZ from stimulated coronal
886 sections of mice in panel B. Identical settings from same brain section were used for imaging. Red
887 arrows represent DCX^+ neuroblasts around subep-$ChAT^+$ neurons.

888 (D) P-S6 intensity analysis of subep-$ChAT^+$ neurons in ipsilateral side (inhibition) vs. contralateral
889 side (control). P = 0.0038, n=8, Paired t-test. Data collected from three stimulated *Cr-Cre* mice.
890 Each dot represents a Subep-$ChAT^+$ neuron.

891 (E) DCX (grey) immunofluorescence staining of ipsilateral SVZ (left image; inhibition) vs.
892 contralateral SVZ (right image; control) from stimulated coronal section of mice in panel C.
893 Identical settings from same brain section were used for imaging. Red arrow displays DCX^+ cells
894 adjacent to subep-$ChAT^+$ neurons in ventral domain of the stimulated and control sides.

895 (F) Analysis of DCX^+ cells in stimulated coronal sections of ipsilateral side (inhibition) vs.
896 contralateral side (control). P<0.0001, n=9, Paired t-test. Data collected from four stimulated *Cr-*
897 *Cre* mice. Each dot represents a total DCX^+ cells per coronal section.

898 (G) Experimental design of *in vivo* optogenetic inhibition for one day post AAV_hSyn1-SIO-
899 stGtACR2-FusionRed virus injection into ipsilateral Cg1 and optical fiber implantation into Cg1
900 regions of P28 *Cr-Cre* mice.

901 (H) EdU (purple), ChAT (green) and pEGFR (grey) immunofluorescence staining of (H')
902 ipsilateral SVZ wholemount (inhibition) (upper images; V-SVZ and lower images; SVZ) vs. (H'')
903 contralateral SVZ wholemount (control) (upper images; V-SVZ and lower images; SVZ) from
904 stimulated mice in panel G. Identical settings from same brain section were used for imaging. Blue
905 arrows display $EdU^+/pEGFR^+$ cells surrounding subep-$ChAT^+$ neurons in V-SVZ and SVZ. Red
906 arrows display $EdU^+/pEGFR^-$ cells surrounding subep-$ChAT^+$ neurons in V-SVZ and SVZ.

907 (I) Left: Analysis of $EdU^+/pEGFR^+$ cells in ipsilateral (inhibition) V-SVZ vs. contralateral
908 (control) V-SVZ of SVZ wholemounts. P = 0.039, n=13, Unpaired t-test. Data collected from four
909 stimulated *Cr-Cre* mice. Each dot represents the total $EdU^+/pEGFR^+$ cells surrounding a subep-
910 $ChAT^+$ neuron.

911 Right: Analysis of $EdU^+/pEGFR^+$ cells in ipsilateral (inhibition) SVZ vs. contralateral (control)
912 SVZ of SVZ wholemounts. P = 0.0006, n=13, Unpaired t-test. Data collected from four stimulated
913 *Cr-Cre* mice. Each dot represents total $EdU^+/pEGFR^+$ cells surrounding a subep-$ChAT^+$ neuron.

914 All error bars indicate SEM.

915

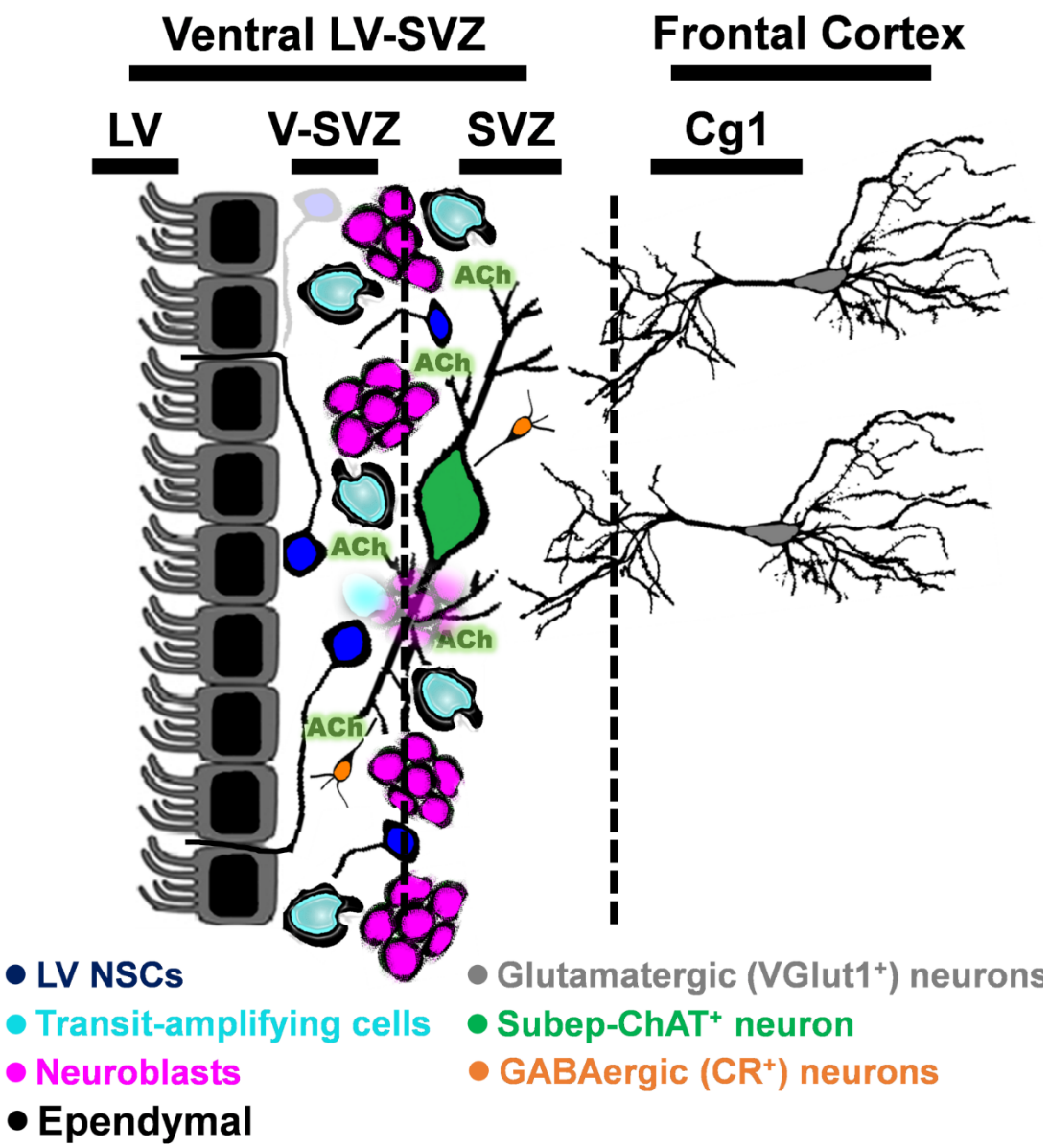

Figure 9 Schematic summary of presynaptic inputs into subep-ChAT^{+} neuron within LV-SVZ niche.